HHS Public Access

Author manuscript

Cell. Author manuscript; available in PMC 2019 April 05.

Published in final edited form as:

Cell. 2018 April 05; 173(2): 470–484.e18. doi:10.1016/j.cell.2018.02.048.

B cell-specific diversion of glucose carbon utilization reveals a unique vulnerability in B cell malignancies

Gang Xiao[1], **Lai N. Chan**[1], **Lars Klemm**[1], **Daniel Braas**[2], **Zhengshan Chen**[1], **Huimin Geng**[3], **Qiuyi Chen Zhang**[1], **Ali Aghajanirefah**[1], **Kadriye Nehir Cosgun**[1], **Teresa Sadras**[1], **Jaewoong Lee**[1], **Tamara Mirzapoiazova**[1], **Ravi Salgia**[1], **Thomas Ernst**[4], **Andreas Hochhaus**[4], **Hassan Jumaa**[1], **Xiaoyan Jiang**[5], **David M. Weinstock**[6], **Thomas G. Graeber**[2], and **Markus Müschen**[1,3,7]

[1]Department of Systems Biology, Beckman Research Institute, and City of Hope Comprehensive Cancer Center, Monrovia, CA 91016

[2]Department of Molecular and Medical Pharmacology, UCLA Metabolomics Center and Crump Institute for Molecular Imaging, University of California Los Angeles, Los Angeles CA 90095

[3]Department of Laboratory Medicine, University of California San Francisco, San Francisco, CA 94143

[4]Abteilung Hamatologie-Onkologie, Klinik fur Innere Medizin II, Universitatsklinikum Jena, Jena, Germany

[5]Terry Fox Laboratory, British Columbia Cancer Agency and Department of Medical Genetics, University of British Columbia, Vancouver, BC, Canada

[6]Dana Farber Cancer Institute and Harvard Medical School, Boston, MA 02215

[7]Lead contact

SUMMARY

B-cell activation during normal immune responses and oncogenic transformation impose increased metabolic demands on B-cells and their ability to retain redox homeostasis. While the serine/threonine-protein phosphatase 2A (PP2A) was identified as tumor suppressor in multiple types of cancer, our genetic studies revealed an essential role of PP2A in B-cell tumors. Thereby, PP2A

For Correspondence: Markus Müschen, MD-PhD, mmuschen@coh.org, Phone: +1-626-218-5171; Gang Xiao, PhD, gaxiao@coh.org, Phone: +1-626-218-5172, Department of Systems Biology, Beckman Research Institute, 1218 South Fifth Ave, Monrovia, CA 91016.

AUTHOR CONTRIBUTIONS.

M.M. conceived the study. G.X. and M.M. wrote the paper and designed experiments. G.X., L.N.C., L.K., D.B., Z.C., Q.C.Z., A.A., K.N.C., T.S., J.L. and T.M. performed experiments and analyzed data. H.G. performed biostatistical analyses. T.G.G. performed analysis and provided expertise in metabolomics. R.S. provided expertise in lung cancer cell model. T.E. and A.H. provided patient-derived samples and expertise in CML. D.M.W. provided patient-derived samples and lymphoma expertise. H.J. provided mouse model and expertise in the function of FoxO1 in leukemia. X.J. provided expertise in LB-100 studies.

DECLARATION OF INTERESTS

All authors declare no competing interests.

redirects glucose carbon utilization from glycolysis to the pentose phosphate pathway (PPP) to salvage oxidative stress. This unique vulnerability reflects constitutively low PPP activity in B-cells and transcriptional repression of *G6PD* and other key PPP enzymes by the B-cell transcription factors PAX5 and IKZF1. Reflecting B-cell-specific transcriptional PPP-repression, glucose carbon utilization in B-cells is heavily skewed in favor of glycolysis resulting in lack of PPP-dependent antioxidant protection. These findings reveal a gatekeeper function of the PPP in a broad range of B-cell malignancies that can be efficiently targeted by small molecule inhibition of PP2A and G6PD.

Graphical Abstract

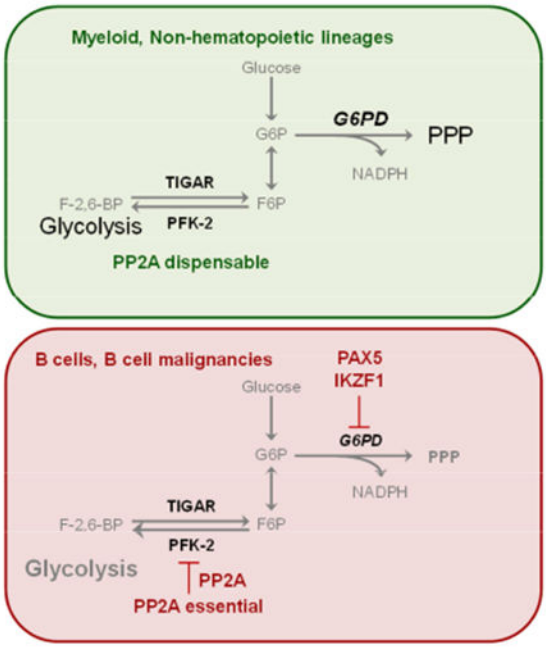

INTRODUCTION

The paradigm of targeted therapy of cancer is based on kinase inhibitors, e.g. the prototypic tyrosine kinase inhibitor (TKI) imatinib for the treatment of BCR-ABL1-driven (*Ph*$^{+}$) leukemias (Hochhaus et al., 2017). Oncogenic signaling frequently involves aberrant activation of kinases, leading to the notion that phosphatases opposing oncogenic kinase signaling have tumor suppressive activity. For instance, the *PTEN* (Li et al., 1997) and *INPP5D* (Lakhanpal et al., 2010) phosphatases are classical tumor suppressors and frequently mutated across multiple types of cancer (http://cancer.sanger.ac.uk/cosmic). Likewise, multiple subunits of the serine-threonine phosphatase PP2A are recurrently deleted or mutated in a wide range of cancer subtypes (Wang et al., 1998), demonstrating that PP2A, like PTEN and INPP5D, represents a tumor suppressor. Recent studies from our group revealed that B cell-derived leukemias are uniquely dependent on PTEN and INPP5D function. Inducible deletion of *Pten* (Shojaee et al., 2016) and *Inpp5d* (Chen et al., 2015) phosphatases in B-lineage leukemia cells caused hyperactivation of B-cell receptor (BCR)-related tyrosine kinases, which mimics overwhelming signaling strength from an

autoreactive BCR (Müschen 2018). Despite malignant transformation, B-lymphoid leukemia cells fully retain their sensitivity to negative selection and cell death at autoimmunity checkpoints. Interestingly, besides PTEN and INPP5D, also PP2A functions as a critical regulator of negative selection and autoimmunity (Apostolidis et al., 2016; Sharabi et al., 2017). Because of its role in cancer and autoimmunity, we studied here the function of PP2A in normal B cells and B-cell malignancies.

RESULTS

B-cell lineage-specific effects of PP2A ablation

PP2A functions as a dimeric holoenzyme composed of a scaffolding subunit A and a catalytic subunit C, which often associates with the regulatory subunit B. As a model for loss of PP2A holoenzyme activity, we studied here genetic ablation of the *Ppp2r1a* gene encoding the PP2A scaffold subunit Aα (PP2A Sub A), which is essential for PP2A activity (Ruediger et al., 2011). To test the function of PP2A in normal B-cell development and B-lymphoid leukemia and lymphoma, we crossed mice carrying floxed *Ppp2r1a* alleles (Ruediger et al., 2011) with the *Mb1*-Cre deleter strain (Hobeika et al., 2006). Genotyping of flow-sorted early B-cells from *Ppp2r1a*$^{fl/fl}$ *Mb1*-Cre mice confirmed efficient Cre-mediated deletion from fraction B (pro-B-cell stage; Figure S1A). Heterozygous *Ppp2r1a*$^{+/fl}$ *Mbl*-Cre mice were phenotypically normal and studied as normal control. Phenotypic analyses of bone marrow and splenic B-cell populations revealed normal pro-B (fraction B) and early pre-B-cell (fraction C) numbers in *Ppp2r1a*$^{fl/fl}$ *Mb1*-Cre mice. However, B-cell populations were diminished by >10-fold once they reached pre-B-cell receptor (pre-BCR)-dependent stages of development (Buchner et al., 2015; fraction C'; Figure 1A-B). Mature splenic B-cells were barely detectable upon deletion of *Ppp2r1a* and numbers were reduced by >20-fold, suggesting that PP2A is also required for survival of mature B-cells (Figure 1C). These results indicate a stage-specific function of PP2A throughout pre-BCR- and BCR-dependent stages of B-cell development. Detailed flow cytometry analyses revealed that ablation of *Ppp2r1a* resulted in selective loss of pre-BCR- (μ-heavy chain) and BCR- (IgM, IgD, Igk) dependent B-cell populations (Figure 1D). Cre-mediated deletion of *Ppp2r1a* not only abrogated expression of the PP2A scaffold Sub A but also destabilized protein expression of catalytic Sub C (Figure 1E; Chen et al., 2005). Conversely, retroviral expression of Sub A rescued normal expression levels of both Sub A and Sub C despite Cre-mediated deletion of *Ppp2r1a.* While Cre-mediated deletion of *Ppp2r1a* reduced enzymatic PP2A activity to background levels, retroviral expression of *Ppp2r1a* (Sub A) increased PP2A enzymatic activity by 7-fold (Figure 1F-G). Inducible ablation of *Ppp2r1a* under cell culture conditions resulted in acute cell death of both pre-BCR$^+$ early and BCR$^+$ mature B-cells (Figure 1H). Interestingly, inducible activation of Cre in *Ppp2r1a*$^{fl/fl}$ myeloid progenitor cells from the same mice had no deleterious effect and slightly increased survival and proliferation, suggesting that dependency on PP2A function is B-cell-specific (Figure 1H). To directly validate that PP2A regulates cell survival in a strict B-cell lineage-dependent manner, *Ppp2r1a*$^{fl/fl}$ B-cell acute lymphoblastic leukemia (ALL) cells were reprogrammed into the myeloid lineage by inducible overexpression of the myeloid transcription factor C/EBPα (Figure 1I; Xie et al., 2004). While deletion of *Ppp2r1a* in CD19$^+$ B-ALL cells caused acute

cell death, viability of $CD11b^+$ C/EBPα-reprogrammed myeloid leukemia cells remained unchanged (Figure 1I).

B-ALL cell survival requires PP2A activity.

Inducible ablation of *Ppp2r1a* induced rapid depletion of both *BCR-ABL1* and $NRAS^{G12D}$ driven B-ALL cells (Figure S1B-C) and suppressed colony forming ability by >10-fold (Figure 2A-B). Conversely, overexpression of *Ppp2r1a* (Sub A) increased competitive fitness and induced outgrowth of Sub A-overexpressing cells (Figure 2C). Likewise, Sub A-overexpression quadrupled the number of colonies formed after plating in semisolid methylcellulose (Figure 2C). Loss of colony formation capacity upon *Ppp2r1a* deletion is consistent with DNA-damage (H2AX-phosphorylation) and activation of Arf and p53 (Figure 2D-E). Ablation of *Ppp2r1a* increased cell death but only slightly affected the cell cycle of B-ALL cells (Figure S1D-G). Mirroring the apoptotic phenotype of B-ALL cells upon *Ppp2r1a* deletion, upregulation of p53 was paralleled by downregulation of Bcl2 (Figure 2D). Taken together, these genetic *in vitro* studies show that PP2A activity is critical for the survival of B-ALL cells.

Functional consequences of PP2A deletion in B-ALL cells

To study the mechanistic basis of the unexpected dependency of B-ALL cells on PP2A enzymatic activity, we determined the biochemical consequences of *Ppp2r1a*-deletion. Measurement of changes of the phosphorylation status of signaling molecules in a phospho-protein array revealed moderately increased phosphorylation of Erk and Akt in response to *Ppp2r1a*-deletion (Figure S2A). Increased activation of PI3K and AKT-mTOR may indeed contribute to toxicity upon deletion of *Ppp2r1a*, because inhibition of PI3K (Idelalisib) and mTOR (Rapamycin) signaling partially rescued cell death in response to *Ppp2r1a*-deletion (Figure S2B-D). Downstream of AKT, deletion of *Ppp2r1a* not only increased activation of mTOR-S6 kinase signaling but also massive phosphorylation and inactivation of FoxO1 and FoxO3a (Figure S3A), which are important mediators of redox equilibrium (Nemoto, 2002). To elucidate the significance of FoxO1- and FoxO3a-phosphorylation and inactivation, we determined the effects of inducible *Foxo1*-deletion in B-cell ALL cells. FoxO factors negatively regulate B-cell proliferation and are inactivated by AKT-mediated phosphorylation (Yusuf et al., 2004). However, tamoxifen-inducible deletion of *Foxo1* in BALL cells abrogated colony formation and caused acute cell death (Figure S4B-C). These findings demonstrate an important role of *Foxo1* in B cell leukemogenesis.

Antioxidant protection in B cells depends on PP2A-function

Since FoxO proteins promote an antioxidant transcriptional program (Nogueira et al., 2008), we examined whether *Ppp2r1a*-deletion affects antioxidant functions of transformed B cells. Multiple antioxidant genes including several known FoxO targets (catalase, *Cat*; superoxide dismutase 2, *Sod2*) were down-regulated upon inducible *Ppp2r1a* deletion (Figure 2F). Gene set enrichment analyses showed a global reduction of expression levels for antioxidant genes ($P<0.01$; Table S1 and Figure S3F), which was paralleled by intracellular accumulation of ROS (8-fold increased; Figure 2G). For functional validation of a potential mechanistic contribution of FoxO factors and the antioxidant catalase, we performed rescue experiments based on overexpression of constitutively active Foxo1 and Foxo3a as well as catalase. *Cat*-

overexpression conferred a significant survival advantage upon inducible *Ppp2r1a* deletion (Figure 2H-I). In contrast, overexpression of constitutively active Foxo1 and Foxo3a mutants was toxic in B-ALL cells regardless of PP2A-ablation (Figure S3D-E). Since PP2A-mediated activation of Foxo1 induces apoptosis through activation of Bim (Yan et al., 2008), overexpression of catalase may predominantly mediate antioxidant protection while Foxo1 and Foxo3 exacerbate the pro-apoptotic phenotype of B-ALL cells upon deletion of *Ppp2r1a*.

Validation of PP2A as therapeutic target in B cell lineage leukemia

To test whether ablation of *Ppp2r1a* is sufficient to prevent development of B-ALL in an *in vivo* setting, *Ppp2r1a*$^{fl/fl}$ *BCR-ABL1*- and *NRAS*^{G12D}-driven B-ALL cells were intravenously injected into sublethally irradiated NOD-scid *Il2rg*$^{-/-}$ (NSG) mice in the presence or absence of Cre (Figure 2J-K). *In vivo* leukemogenesis was monitored through bioimaging of luciferase labeled ALL cells (Figure 2L). In line with *in vitro* results, recipient mice injected with *Ppp2r1a*$^{fl/fl}$ B-ALL cells showed reduced leukemia burden upon deletion of *Ppp2r1a* and significantly prolonged overall survival in both *BCR-ABL1*- and *NRAS*^{G12D}-driven B-ALL models (Figure 2J-K). To determine whether mice in the *Ppp2r1a*$^{fl/fl}$ +Cre group succumbed to leukemia because B-ALL can develop in the absence of PP2A (B-ALL with deleted *Ppp2r1a* alleles) or because some B-ALL clones escaped Cre-mediated deletion (B-ALL retaining *Ppp2r1a* alleles), we studied the genotype of B-ALL cells that were isolated from enlarged spleens when the mice were euthanized (Figure 2M). Genomic and protein expression studies revealed that in all 7 cases, B-ALL developed from *Ppp2r1a*$^{fl/fl}$ clones that evaded Cre-mediated deletion and expressed normal levels of PP2A. Given that <0.1% of Cre-GFP^{+} cells escape deletion, these findings demonstrate the strong selective pressure in favor of B-ALL clones that retained *Ppp2r1a*$^{fl/fl}$ alleles.

PP2A restricts glycolytic activity in B-lymphoid but not myeloid leukemia cells

AMPK is negatively regulated by PP2A (Wu et al., 2007) and the active phospho-AMPK-T^{172} was identified among the upregulated phosphoproteins upon *Ppp2r1a*-deletion (Figure S2A). We recently found that AMPK-activation in B-ALL cells promotes glycolysis (Chan et al., 2017), suggesting that PP2A negatively regulates glycolysis in B cells. Here we showed that inducible deletion of *Ppp2r1a* amplified mTORC1 signaling (Figure S3A), which was previously shown to stimulate glycolysis as a result of PI3K signaling (Düvel et al., 2010). For this reason, we studied the impact of *Ppp2r1a*-deletion on glucose and energy metabolism in B-cell and myeloid lineage leukemias. Inducible ablation of *Ppp2r1a* in B cells substantially increased glucose consumption, ATP levels and lactate production (by 3-fold; Figure S4A). Seahorse metabolic analysis revealed that *Ppp2r1a*-deletion increased glycolytic activity in B-lymphoid but not myeloid leukemia cells (Figure 3A-B). Mitochondrial respiration remained unchanged after *Ppp2r1a*-deletion in both B-lymphoid and myeloid leukemia cells (Figure S4B-C). While glycolysis primarily generates metabolic intermediates and ATP, the pentose phosphatase pathway (PPP) has a critical antioxidant function to generate reducing equivalents, in the form of NADPH (Cairns et al., 2011). Reduced nicotinamide adenine dinucleotide phosphate (NADPH) represents a critical product of the PPP and has important reducing potential to maintain redox balance (Patra and Hay, 2014). For instance, NADPH can reduce glutathione disulfide (GSSG) to the

sulfhydryl form glutathione (GSH), which can salvage oxidative stress (Cairns et al., 2011). In addition, the PPP is critical for DNA replication in proliferating leukemia cells and generates ribose 5-phosphate (R5P), used in the *de novo* synthesis of ribonucleotides and later nucleic acids.

PP2A is required to redirect glucose carbon utilization towards the pentose phosphate pathway in B cells

We examined how loss of PP2A activity affected glucose utilization via glycolysis relative to PPP in B-ALL cells. To trace the activity of glycolysis relative to the PPP pathway upon *Ppp2r1a*-deletion, we performed mass spectrometry-based metabolite profiling and carbon fate analyses based on ^{13}C isotopic labels. Carbon fate tracing showing the M1 and M2 isotopomer distribution of lactate derived from [1,2-^{13}C] glucose was used to distinguish ^{13}C atoms directly passing through the glycolytic pathway (M2) from ^{13}C atoms passing through the oxidative arm of the PPP and cycled back to glycolysis (M1). Interestingly, *Ppp2r1a*-deletion significantly reduced overall carbon utilization through the PPP in B-lymphoid cells (Figure 3C) while the distribution of M1 (PPP) and M2 (glycolysis) ^{13}C atoms remained unchanged when *Ppp2r1a* was deleted in B→Myeloid reprogrammed cells (Figure 3D; inducible expression of *Cebpa*). A detailed analysis of individual glycolysis (M2) and PPP (M1) metabolites revealed that *Ppp2r1a*-deletion in B-lymphoid cells strongly increased labeling of ^{13}C atoms in multiple glycolytic intermediates (in particular F-1,6-BP) while carbon labeling was consistently reduced for all PPP metabolites studied (Figure 3C). Conversely, for B→Myeloid reprogrammed cells, inducible deletion of *Ppp2r1a* had only minor effects and caused modest stimulation of ^{13}C atoms through both glycolytic (M2) and PPP (M1) intermediates (Figure 3D).

PP2A regulates glucose carbon utilization in B cells at the level of Pfkfb2

The relative contribution of glycolysis and PPP flux is controlled by the bifunctional 6-phosphofructo-2-kinase/fructose 2,6-bisphosphatase 2 (Pfkfb2) kinase or phosphatase activity (Ros and Schulze, 2013). Importantly, *Ppp2r1a*-deletion in B cells but not myeloid cells increased phosphorylation of Pfkfb2 at S-483 (Figure 3E), which promotes Pfkfb2 kinase (6-phosphofructo-2-kinase; PFK-2) at the expense of its phosphatase activity (Pozuelo Rubio et al., 2003). The consequence of enhanced PFK-2 activity is allosteric activation of the rate-limiting enzyme PFK-1 which catalyzes the conversion of fructose-6-phosphate (F6P) to fructose-1,6-bisphosphate (F-1,6-BP) and thereby promotes glycolysis at the expense of the PPP. While F6P can still be utilized in the PPP via G6P as substrate for G6PD, F-1,6-BP is committed to the glycolysis pathway and gives rise to lactate. These findings suggest that PP2A regulates the phosphorylation status of Pfkfb2-S^{483} and, thereby, a critical metabolic switch between glycolysis and PPP. Indeed, massively increased S-483 phosphorylation of Pfkfb2 following *Ppp2r1a* deletion (Figure 3E), redirects glucose carbon flux from the PPP to glycolysis pathway (Ros et al. 2012). Functional consequences of this switch in B cells include increased utilization of glycolysis at the expense of the PPP (Figure 3F), >20-fold increased conversion of F6P to F-1,6-BP (Figure 3G), reduced NADPH/NADP ratios (Figure 3H). Consistent with diminished NADPH/NADP ratios, inducible deletion of *Ppp2r1a* substantially decreased GSH/GSSG ratios, indicating exhaustion of reductive reserves in B cells upon loss of PP2A function (Figure 3I). Interestingly, none of

these changes occurred in myeloid cells. While patient-derived B cell leukemia and lymphoma cells express PP2A protein at high levels, protein levels for PP2A subunit C are much lower in myeloid leukemia samples (Table S2-S4) and virtually undetectable for PP2A subunit A (Figure 3J). PP2A expression levels in B-cell and myeloid leukemia match the phosphorylation status of Pfkfb2-S^{483} (Figure 3E), which provides an explanation for the strikingly different outcome of PP2A-deletion in B cell- and myeloid leukemia cells.

The fructose-2,6-bisphosphate 2-phosphatase TIGAR efficiently rescues cell death upon deletion of PP2A

The TP53 Induced Glycolysis Regulatory Phosphatase (TIGAR) can reverse the effects of PFKFB2 S-483 phosphorylation and stimulate carbon flux through the pentose phosphate pathway (PPP) at the expense of glycolysis (Bensaad et al., 2006; Cheung et al., 2013). For this reason, we tested the ability of Tigar overexpression (Figure 4A-B) to rescue cell death upon inducible ablation of *Ppp2r1a* in B-cell ALL. In BALL cells with intact PP2A expression, overexpression of Tigar resulted in a minimal survival advantage. However, when *Ppp2r1a* was deleted by inducible expression of Cre, overexpression of Tigar rescued BALL cells from cell death and induced a strong survival advantage (Figure 4C-D). Inducible deletion of *Ppp2r1a* in B-cell ALL substantially decreased NADPH/NADP ratios (Figure 4E). As expected, normal NADPH/NADP ratios were restored by reconstitution of *Ppp2r1a* expression using a retroviral overexpression vector (compared to empty vector, EV; Figure 4E). Overexpression of Tigar in B-ALL cells with intact PP2A-function induced a slight increase of NADPH/NADP ratios. Inducible deletion of *Ppp2r1a* substantially decreased NADPH/NADP ratios, which was fully restored by Tigar overexpression, comparable to restoration of *Ppp2r1a* itself (Figure 4F). The important role of TIGAR in the diverting glucose carbon flux from glycolysis to the PPP (Bensaad et al., 2006; Cheung et al., 2013) and the ability of Tigar overexpression to fully substitute for PP2A (Figure 4) support the concept that PP2A serves an essential role in the survival of B cells by balancing carbon utilization of glycolysis versus PPP. Given the complexity of redox regulation, it is likely that factors other than PPP also contribute to loss of NADPH upon *Ppp2r1a* deletion of in B cells.

PP2A and pentose phosphate pathway enzymes represent B-cell specific vulnerabilities

Recent work by our group showed that genetic lesions of *PTEN* occur throughout virtually all types of human cancer with the exception of B-ALL (Shojaee et al., 2016). Likewise, we found that mutations and deletions of *PPP2R1A* occur frequently throughout multiple cancer types of cancer but were not detected in B-ALL and B cell lymphoma. In solid tumors across 16 types of cancer (23,009 samples studied) we found genetic lesions of *PPP2R1A* on average in 3% of cases studied (range 0.5 to 14%). On the other hand, genetic lesions of *PPP2R1A* were also found in myeloid leukemia (187 samples studied) but not in B cell leukemia and lymphoma (323 samples studied; Figure S5A). These genetic findings show that malignant clones in B cell tumors are -unlike other types of cancer- not positively selected for loss of PP2A function. On the premise that PP2A regulates a central metabolic switch between glycolysis and PPP, we studied expression levels of glycolysis and PPP-related enzymes in B-cell compared to myeloid malignancies (Figure S4D; Figure S5B). Studying 807 B-lymphoid leukemia patient samples and 355 myeloid samples, we found

substantially higher mRNA levels of glycolytic PFK-1 enzymes in B-lymphoid compared to myeloid samples (*PFKL*, P<0.0001; *PFKM*, P=0.0091; *PFKP*, P<0.0001). Interestingly, while we did not detect mutations in PP2A subunits, we found 19 somatic mutations in PFK-1 enzymes in a panel of 56 BALL and B cell lymphoma cell lines (Table S5). Conversely, mRNA levels of PPP enzymes were substantially downregulated in B-lymphoid compared to myeloid samples (*G6PD*, *PGD*, *RPIA*, *RPE*, *TKT* and *TALDO1*, P<0.0001 for each gene; Figure S4D). Glucose-6-phosphate dehydrogenase (G6PD) and 6-phosphogluconate dehydrogenase (PGD) catalyze the rate-limiting steps of PPP and promote PPP relative to glycolysis (Hitosugi et al., 2012; Lin et al., 2015). Compared to normal myeloid progenitor cells (n=43) and myeloid leukemia (n=484), mRNA levels of *G6PD* are low in normal (n=47) and malignant (n=405) B cell populations (Figure S5B).

B-lymphoid transcription factors repress G6PD and PPP activity

Cebpa-mediated reprogramming of B cells into the myeloid lineage gradually increased mRNA and protein levels of G6PD and PGD (Figure 5A-B). ChIP-seq data from human B-cells showed enriched binding of these B-lymphoid transcription factors on *G6PD* promoters, which was confirmed by single-locus quantitative ChIP (Figure 5C-D). The B-lymphoid transcription factors PAX5 and IKZF1 negatively regulate glucose uptake and are frequently deleted in B-lineage ALL (Chan et al., 2017). Interestingly, restoration of PAX5 expression in a *Pax5*-deficient mouse model of B-lineage ALL (Liu et al., 2014) significantly repressed G6pdx and G6pd2 expression levels (Figure 5E). Likewise, restoration of PAX5 and IKZF1 in *PAX5*- and *IKZF1*-deficient patient-derived B-lineage ALL xenografts reduced G6PD by >50-fold to levels at or below the detection limit (Figure 5F). In some cases, genetic lesions of PAX5 and IKZF1 result in expression of dominant-negative (DN) transcription factors (*PAX5-ETV6*; intragenic deletion of *IKZF1* zinc fingers). Overexpression of DN-PAX5 and DN-IKZF1 in patient-derived B-lineage ALL xenografts expressing functional PAX5 and IKZF1 induced strong upregulation of G6PD (Figure 5F) demonstrating that functional G6PD deficiency in B cells is the result of B cell-specific transcriptional repression. Interestingly, higher than median expression levels of *G6PD* are associated with poor clinical outcome and shorter overall survival in all four clinical trials that we studied for patients with B cell lymphomas but not in patients with acute myeloid leukemia (Figure 5G-H).

Studying PP2A and G6PD protein levels in patient-derived B-ALL (n=4), diffuse large B cell lymphoma (DLBCL; n=2) and mantle cell lymphoma (MCL; n=3) xenografts, we confirmed that B cell tumors generally express high levels of PP2A subunit A and C and low levels of the PPP rate-limiting enzyme G6PD compared to patient-derived myeloid leukemia samples (n=10; Figure 3J). These findings suggest that B-cell intrinsic repression of the rate-limiting PPP enzyme G6PD may serve as a gatekeeper function to safeguard against malignant transformation, while higher expression levels of G6PD are associated with a more aggressive course of disease in B-cell malignancies. To test whether G6PD was sufficient to rescue inducible ablation of *Ppp2r1a* in B-cell ALL cells, we overexpressed murine G6pdx and human G6PD and verified increased expression levels by Western blot (Figure S6A). Unlike TIGAR, which redirects carbon glucose flux from glycolysis to the PPP, the PPP key enzyme G6PD (murine G6pdx and human G6PD) was not sufficient to

rescue B-ALL cell death upon inducible deletion of *Ppp2r1a* (Figure S6B-C). This is a central difference from TIGAR (Figure 4), which unlike G6PD has no direct function in the PPP but controls supply of the PPP with glucose carbon flux (Bensaad et al., 2006).

Transcription factors that determine B cell identity regulate PPP-activity and dependency on PP2A

We tested here the hypothesis that B cell-specific transcription factors are responsible for low PPP activity in B cells, hence PP2A as a B cell-specific vulnerability. To this end, we replaced the four stem cell factors Oct4, Sox2, Nanog and Myc in a vector that was previously used to generate iPS cells (Takahashi & Yamanaka 2006) with the four B cell transcription factors Pax5, Ikaros, Ebf1 and Tcf3. Inducible activation of this polycistronic vector in human embryonic kidney cells resulted in expression of all four B-lymphoid transcription factors and substantial reduction of NADPH/NADP ratios (Figure 6A-B). In addition, doxycycline-inducible expression was sufficient to reprogram murine myeloid leukemia cells into B cells (Figure 6C-D). Myeloid→B cell reprogramming downregulated G6PD and upregulated PP2A (Figure 6 E) and hence recapitulated metabolic characteristics of B cells (Figure 3J). In a third approach, we studied small cell lung cancer cells (SCLC). Unlike other types of lung cancer, SLCL cells often aberrantly express PAX5 (Kanteti et al. 2009). Compared to $PAX5^-$ SCLC (e.g. DMS273), $PAX5^+$ SCLC (e.g. H69) cells expressed G6PD at low and PP2A at high protein levels, respectively (Figure 6F), and had much lower NADPH/NADP ratios (Figure 6G). Interestingly, lentiviral expression of PAX5 in $PAX5^-$ SCLC (DMS273) reduced NADPH/NADP ratios down to levels in $PAX5^+$ SCLC cells (H69). Overexpression of PAX5 in SCLC (H69) reduced NADPH/NADP ratios even further (Figure 6G). These effects depend on PAX5 and likely other B-lymphoid transcription factors and can occur in non-B cells (e.g. kidney, myeloid and SLCL cells) when PAX5 is aberrantly expressed. While not the focus of this study, these findings suggest a previously unexplored rationale for specific targeting of PP2A and G6PD in SCLC cells.

Target validation of PP2A in human B cell malignancies.

In proof-of-concept experiments, we have tested here the PP2A small molecule inhibitor LB-100 (4-Methylpiperazin-1-yl-7-oxabicyclo-heptane-2-carboxylic acid) and the G6PD-inhibitor by 6-aminonicotinamide (6-AN; Figure S7A) in B cell leukemia and lymphoma samples. LB-100, the first-in-class PP2A inhibitor studied here is currently in two clinical trials (NCI designated NCT03027388 and NCT01837667). A phase 1 safety study with 7 dose-escalations did not note relevant toxicity (Chung et al., 2017). LB-100 is a water-soluble small molecule inhibitor of PP2A (IC_{50} 0.9 μmol/l) and was initially designed to sensitize solid tumors to chemotherapy (Lu et al., 2009). To document feasibility, we injected C57B/6J mice with LB-100 (1.5 mg/kg) five times over the course of 9 days and monitored PP2A inhibition in normal T cell subsets (Figure S7C-E) and myeloid subsets, which showed minimal impact. Interestingly, a recent study showed that proarthritogenic T cells in rheumatoid arthritis are dependent on PPP-mediated antioxidant protection (Yang et al., 2016), suggesting that targeting of PP2A alone or in combination with G6PD may be useful for these patients. Here we used LB-100 to study pharmacological PP2A ablation in the context of Pax5 and Ebf1 haploinsufficiency (hemizygous *Pax5* and *Ebf1* deletions). To this end, $Pax5^{+/-}Ebf1^{+/-}$ B-ALL cells and wildtype control B-ALL cells were treated with

LB-100 at the concentrations indicated and cell viability was measured. Interestingly, partial or complete loss of B cell-specific transcription factors (e.g. *Pax5* and *Ebf1*) relieved dependency on PP2A and resulted in reduced sensitivity to LB-100 in B cells (Figure 6H).

CRISPR/Cas9-mediated genetic ablation of PPP2R1A in patient-derived B-cell ALL

We transduced patient-derived Ph^+ ALL cells with inducible Cas9 and three different guide-RNAs directed against *PPP2R1A* and a non-targeting guide (Figure 7A; Table S6). Western blot analysis revealed that deletion of *PPP2R1A* was achieved at varying levels. The extent of *PPP2R1A* deletion correlated with loss of the catalytic PP2A subunit C and phosphorylation of H2AX (S139; Figure 7A). Compared to patient-derived Ph^+ ALL cells carrying Cas9 and a non-targeting guide RNA, three different guide-RNAs directed against *PPP2R1A* induced depletion of B-ALL cells from cell culture (Figure 7B and S7B), confirming dependency of patient-derived B-ALL cells on PP2A function.

Feasibility and efficacy of pharmacological PP2A inhibition in B cell malignancies.

Studying biochemical activity of LB-100 in patient-derived Ph^+ ALL cells, we found that near-complete loss of PP2A activity at 5 μmol/l (Figure 7C) was paralleled by strong activation of AKT-mTOR signaling and H2AX-phosphorylation (Figure 7D), which is consistent with increased ROS-levels in patient-derived Ph^+ ALL cells (Figure 7E). Consistent with lineage-specific effects of *Ppp2r1a* deletion (Figure 1I), LB-100 selectively induced cell death in B-cell leukemia and lymphoma PDX but not myeloid leukemia cells (CML, AML; Figure 7F-H). Owing to B-lymphoid transcriptional repression of G6PD and other central PPP enzymes (Figure 5A-F), B cells are uniquely vulnerable to PPP inhibition. In agreement with these results, we found that pharmacological inhibition of G6PD by 6-AN further exacerbated B cell-intrinsic G6PD deficiency and induced cell death in B-cell leukemia and lymphoma but not myeloid leukemia cells (Figure 7I). Interestingly, combination studies of LB-100 and 6-AN revealed that direct (6-AN via G6PD) and indirect (LB-100 via PP2A) inhibition of PPP strongly synergized in patient-derived Ph^+ ALL, mantle cell lymphoma and DLBCL cells (Figure 7J-L; Table S7). To test this therapeutic concept in a preclinical transplant experiment, we injected patient-derived DLBCL cells (Table S3) carrying concurrent *MYC* and *BCL2* gene rearrangements into NSG mice and treated the mice with LB-100 (1.5 mg/kg), 6-AN (1 mg/kg) or a combination of both via i.p. injections. The Kaplan-Meier analysis on day 50 showed a significant difference in survival for the LB-100 (P=0.0005) or LB-100 +6AN (P=0.0002) arms compared to vehicle controls (Figure 7M; Log-rank test). In summary, we propose that targeting of PP2A in B-cell malignancies is immediately translatable given the evidence supporting safety of LB-100. Our studies provide a strong rationale for agents that will target PP2A, TIGAR or G6PD as lineage-specific and previously unrecognized vulnerabilities in B cell malignancies (B-ALL and B cell lymphoma).

STAR METHODS

Contact for Reagent and Resource Sharing

Further information and requests for reagents may be directed to and will be fulfilled by the Lead Contact, Markus Müschen (mmuschen@coh.org).

Experimental Model and Subject Details

Cell lines—Leukemia cell lines were maintained in Roswell Park Memorial Institute (RPMI) 1640 medium (GIBCO) with GlutaMAX supplemented with 10-20% fetal bovine serum (FBS), 100 IU/ml penicillin and 100 μg/mL streptomycin (GIBCO). Small cell lung cancer cell lines provided by Dr. Ravi Salgia, were cultured in the same condition as for leukemia cell lines. All cell lines were cultured at 37°C in a humidified incubator with 5% CO_2. All cell lines were tested to be mycoplasma free by MycoAlert PLUS kit (LONZA).

Patient-derived B-ALL and B-cell lymphoma samples—Patient samples were obtained in compliance with the internal review board of the Beckman Research Institu te of City of Hope. Patient samples were collected from biopsy of ALL (bone marrow) or lymphoma (periph eral blood) patients at the time of diagnosis or relapse. All samples were transplanted into sublethally irradiat ed NOD.Cg-*Prkdc*^{scid} *Il2rg*^{tm1Wjl}/SzJ (NSG; The Jackson Laboratory) mice through tail vein injection. Aft er collection of cells, lymphoma xenografts were frozen in aliquots and ALL xenografts were cultured on OP 9 stroma cells in Alpha Minimum Essential Medium (MEMα; GIBCO) with GlutaMAX supplemented with 20% FBS, 1mM sodium pyruvate, 100 IU/mL penicillin and 100 μg/mL streptomycin at 37°C in a humidifie d incubator with 5% CO_2. Before experimental usage, all the human xenografts were tested to be mycoplasm a free (MycoAlert PLUS, LONZA).

Murine primary and leukemia cells—Bone marrow and splenic cells were harvested from mice between 6-8 weeks of age without signs of inflammation. After filtration through a 70 μm cell strainer, cells were supplied to lysis buffer based erythrocytes depletion (RBC Lysis Buffer, BioLegend). Resuspended cells were then used for further experiments. Bone marrow cells were cultured in Iscove's Modified Dulbecco's Medium (IMDM; GIBCO) with GlutaMAX supplemented with 20% FBS, 100 IU/ml penicillin, 100 μg/mL streptomycin and 50 μmol/l β-mercaptoethanol (GIBCO). Bone marrow cells, for IL-7-dependent pre-B cell culture were cultured in full IMDM supplemented with 10 ng/ml recombinant mouse IL-7 (PeproTech). To generated murine B-lineage *Ph*$^+$ ALL cell, retroviral transduction of *BCR-ABLI* was performed to cultured pre-B cells. After transformation with BCR-ABL1, ALL cells were cultured in IL-7-withdrawed IMDM. *NRAS*^{G12D} B-ALL cells were selected with puromycin (GIBCO) and were maintained with IL-7 supplemented IMDM. Murine B-ALL cells were cultured no longer than 2 months to avoid accumulation of additional genomic mutations. Murine *BCR-ABL1* B-ALL cells used in 1,2-2^{13}C D-Glucose tracing and metabolites profiling experiments, were cultured in glucose-free DMEM with 20% dialyzed FBS, 100 IU/ml penicillin, 100 μg/mL streptomycin and 50 μmol/l β-mercaptoethanol (GIBCO). The same medium with 25 mmol/l 1,2-2^{13}C D-Glucose (Cambridge Isotope Laboratories, Inc.) was used labeling during a 24 hours interval. For myeloid leukemia (CML-like) cells, the myeloid-specific protocol described previously (Chan et al., 2017) was used. In brief, murine bone marrow cells were cultured in IMDM containing 10 ng/ml recombinant mouse IL-3, 25 ng/ml recombinant mouse IL-6 and 50 ng/ml recombinant mouse stem cell factor (SCF; PeproTech). After BCR-ABL1 mediated transformation, murine CML-like cells were cultured in IMDM without additive cytokines. Lineage-specific characterization of BCR-ABL1-transformed *Ph*$^+$ ALL and CML-like cells was performed by flow cytometry (LSRFortessa, BD Biosciences). Mature splenic B cells

were cultured in IMDM with 20% FBS, 100 IU/ml penicillin, 100 μg/mL streptomycin and 50 μmol/l β-mercaptoethanol (GIBCO), supplemented with 10 ng/ml mouse IL-4 (Pepro Tech), 100 ng/ml human BAFF (Cell Guidance Systems) and 1 μg/ml mouse CD40L (Cell Guidance Systems). After 2 days in cell culture, more than 90% of the cells were $CD19^+$ B cells and were used for further experiments.

Animals—C57BL/6, NOD.Cg-*Prkdc*^{scid} *Il2rg*^{tm1Wjl}/SzJ, *Mb1*-Cre and *Ppp2r1a*$^{fl/fl}$ mice were purchased from The Jackson Laboratory. *Ppp2r1a*$^{fl/fl}$ mice were backcrossed to C57BL/6 background for more than 8 generations. Vav-tTAxTet^{off}-sh*Pax5* mice were obtained from Dr. Ross A. Dickins. For animals bred in house, littermates of the same sex were randomized to experimental groups. All mouse breeding and experiments were subject to institutional approval by the Beckman Research Institute Animal Care and Use Committee.

Method details

Flow cytometry—Cells were washed in PBS and subjected to Fc receptor blocking (TruStain, Biolegend) for 10 min at room temperature. 10^6 cells per ml were used to perform staining with antibodies listed for 15-30 min at 4°C. After washing with PBS, cells were suspended in PBS with propidium iodide (PI, 0.2 μg/mL) or DAPI (0.75 μg/mL) to exclude dead cells. For cell-cycle analysis, the Click-iT EdU Flow Cytometry Assay Kit (Life Technologies) was used according to the manufacturer's instructions. To measure intracellular ROS levels, cells were incubated for 7 min with 1 μmol/L 5-(and-6)-chloromethyl-2',7'-dichlorodihydrofluorescein diacetate, acetyl ester (CM-H_2DCFDA, Life Technologies) at 37°C. After washing with PBS, the cells were incubated for additional 15 min at 37°C in PBS. Fluorescence signals from oxidated CM-H_2DCFDA in viable cells were measured by flow cytometry. All flow cytometry assays were performed on a LSRFortessa (BD Biosciences). All the fluorescence-activated cell sorting procedures were performed on a FACSAria II (BD Biosciences). Flow cytometry data were exported and analyzed with FlowJo (FlowJo, LLC).

Western blotting—PBS washed cells were lysed in CelLytic buffer (Sigma-Aldrich) supplemented with 1% protease inhibitor cocktail (Fisher Scientific). 20 μg of protein lysates per sample were separated on Criterion TGX (Bio-Rad) 4-20% Tris-Glycine extended gradient gels and transferred on nitrocellulose membranes (Bio-Rad). The Western Breeze Immunodetection System (Life Technologies) was used for signal development, and chemiluminescent signal was detected by X-ray film exposure. Primary antibodies used for western blotting are listed below.

PP2A phosphatase activity measurement—2×10^7 leukemia cells were used for measuring PP2A activity following manufacturer's protocol. PP2A Immunoprecipitation Phosphatase Assay Kit (17-313, Millipore) was used to perform this assay.

Reprogramming of leukemia cells from pre-B into myeloid lineage by C/EBPα—*Ppp2r1a*$^{fl/fl}$ *BCR-ABL1* ALL cells were transduced with rtTA C/EBPα. After antibiotic selection, those cells were transduced with Cre-ER^{T2}-GFP or EV. For growth competition

assays, cells were induced with doxycycline for 2 days, 4-OHT (Sigma-Aldrich) was used to induce Cre-ER^{T2} activity. The percentages of GFP$^+$ cells of pre-B (CD19$^+$ CD11b$^-$) and reprogrammed myeloid (CD19$^-$ CD11b$^+$) populations were measured by flow cytometry at the same time. For metabolites extraction, transduced cells were sorted for GFP$^+$ cells before induction. 5 days after induction with doxycycline, reprogrammed cells were used for 1,2-2^{13}C D-glucose tracing and metabolites profiling.

Retroviral and lentiviral transduction—Constructs used for retroviral or lentiviral transduction are listed in the key resources Table. Virus production was performed with HEK-293FT cells (Life Technologies) using Lipofectamine 2000 (Life Technologies). Cells were co-transfected with the plasmid of interest, pHIT60 (gag-pol) and pHIT123 (ecotropic env; kindly provided by Donald B Kohn, UCLA). HEK-293FT cells were cultured in high glucose Dulbecco's modified Eagle's medium (DMEM, GIBCO) with GlutaMAX supplemented with 10% FBS, 100 IU/ml penicillin, 100 μg/ml streptomycin, 25 mM HEPES, 1 mM sodium pyruvate and 0.1 mM non-essential amino acids (GIBCO). 16h after liposomal transfection, cell culture medium was replaced by full grow media, supplemented with 10 mM sodium butyrate. After 8 hours, cell culture medium was replaced with full grow media. 24 hours later, the virus-containing supernatant was collected and filtered through 0.45 μm filters. Cell transduction was performed with RetroNectin (TAKARA) according to manufactures protocol. Lentiviral particles were produced via co-transfection of plasmid of interest with pCD/NL-BH*DDD and EM140 like the retroviral particle production. Antibiotic selection was performed on transduced cells according to the specific antibiotic resistance carried by the respective construct.

Colony forming assay for murine ALL cells—10,000 B-ALL cells were resuspended in 1 mL murine MethoCult medium (M3231 or M3630, STEMCELL Technologies) and cultured in 35 mm dishes at 37°C in a humidified incubator with 5% CO_2. Colony numbers were counted after 7-14 days using an automated colony counter.

NADPH/NADP ratio measurement—2×10^7 cells were harvested and subjected to measure NADPH/NADP ratio by NADP/NADPH Assay Kit (ab65349, Abcam). NADPH/NADP ratios relative to control cells were calculated in each experiment.

Affymetrix GeneChip expression analysis—Total RNA was isolated using the NucleoSpin RNA kit (MACHEREY-NAGEL). RNA quality was determined with the Agilent Bioanalyzer (Agilent Technologies). Biotinylated cRNA was generated and fragmented based on the Affymetrix protocol and hybridized to mouse Gene 1.0 ST (Affymetrix). After scanning (GeneChip Scanner 3000 7G; Affymetrix) of the arrays, the CEL files generated were analyzed using BRB Array Tool (http://linus.nci.nih.gov/BRB-ArrayTools.html) and processed using the RMA algorithm (robust multi-array average) for normalization and summarization. Gene expression ratios were processed and visualized as a heat map utilizing Gene Cluster and Java Treeview. Gene Set Enrichment Analysis (GSEA) was performed using list in Table S1 with GSEA software. Raw data are available via GEO accession number GSE83742.

In vivo* leukemia and lymphoma cell transplantation—Ppp2r1a*$^{fl/fl}$ *BCR-ABL1* B-ALL cells were transduced with retrovirus to overexpress firefly luciferase, selected with puromycin, and then transduced with Cre-IRES-GFP or GFP empty vector. 2 days after transduction, GFP^{+} cells were sorted by FACSAria II (BD Biosciences) and genotyping was performed to verify Cre mediated deletion. 1×10^{6} viable cells were intravenously injected into sublethally irradiated (2 Gy) NSG mice (6-8 weeks old females). Comparable viability and luciferase activity of Cre-IRES-GFP and GFP transduced cells were confirmed by flow-cytometry and D-Luciferin (Gold Bio) induced bioluminescence signal. Leukemia progression in mice was monitored at the times indicated using an *in vivo* IVIS Spectrum bioluminescence/optical imaging system (PerkinElmer Inc). 2.5 mg D-Luciferin (dissolved in PBS) per mouse was injected intraperitoneally 15 min before measuring. General anesthesia was induced with 5% isoflurane and continued during the procedure with 2% isoflurane introduced through a nose cone. *Ppp2r1a*$^{fl/fl}$ *Nras*^{G12D} ALL cells were transduced with Cre-ER^{T2}-IRES-GFP or ER^{T2}-IRES-GFP empty vector. 2 days after transduction, GFP^{+} cells were sorted by FACSAria II (BD Biosciences). 3×10^{6} viable cells after 24 hours' 4-OHT treatment were intravenously injected into sublethally irradiated (2 Gy) NSG mouse (6-8 weeks female). After transplantation, 5 mg/mouse/day Tamoxifen (Sigma-Aldrich) was administrated to recipient mice with *Nras*^{G12D} ALL cells for 7 days through oral gavage. 3×10^{6} viable patient-derived diffuse large B cell lymphoma cells (BOS12; Table S3) were intravenously injected into sublethally irradiated (2 Gy) NSG mouse (6-8 weeks female). Treatment of vehicle, LB-100 (1.5 mg/kg), 6- AN (1 mg/kg) or combination (1.5 mg/kg LB-100 + 1 mg/kg 6-AN) started 7 days after transplantation by intraperitoneal injection. Mice were euthanized when they reached the criteria of terminal sickness caused by leukemia. Bone marrow and spleen cells were collected for flow cytometry analysis. All mouse experiments were subject to institutional approval by the Beckman Research Institute Animal Care and Use Committee. 6-8 weeks old female NSG mice were randomly allocated into each group. The minimal number of mice in each group was calculated by using the 'cpower' function in R/Hmisc package. No blinding was used.

Extracellular glucose, lactate and intracellular ATP measurements—Glucose and lactate levels in cell culture medium were measured with the Amplex Red Glucose/Glucose Oxidase Assay Kit (Life Technologies) and the L-Lactate Assay Kit (Cayman Chemical). Medium at indicated time points was collected and stored at −80°C and were later processed according to the manufacturers' instructions. Intracellular ATP levels were measured using the ATP Bioluminescence Assay Kit CLS II (Roche). Cell pellets were harvested at different time points and processed as instructed by manufacturer's protocol.

Glycolysis and mitochondrial respiration measurements—Seahorse XF^{e}24 extracellular flux analyzer (Agilent Technologies) was used to measure oxygen consumption rate (OCR) and extracellular acidification rate (ECAR) of mouse B-ALL and myeloid leukemia cells. Cells treated with 4-OHT or vehicle at indicated time points were subsequently processed to measure glycolysis and mitochondrial function with Seahorse XF Glycolysis Stress Test and Cell Mito Stress Test Kit (Agilent Technologies). In brief, 1.5×10^{5} cells/well were plated in Cell-Tak (Corning) coated XF 24 micro culture plate (Agilent Technologies). For glycolysis stress assay, cells were incubated in XF-Base

Medium supplemented with GlutaMAX for 1 h at 37°C in non-CO_2 incubator, basal ECAR was then measured at the glucose-deprived stage. After injection of saturated glucose (10 mmol/l), glycolysis induced ECAR was measured. Oligomycin (1 μmol/l) and 2-deoxyglucose (2-DG, 0.1 mol/l) were sequentially injected and realtime ECAR was measured to reflect glycolytic capacity and specific inhibition of glycolysis. Non-glycolytic acidification (glucose deprived), glycolysis and glycolytic capacity were determined. ECAR values were normalized to cell numbers and are shown as fold change relative to non-glycolytic ECAR. Similarly, cells kept in XF-Base Medium supplemented with glucose (10 mmol/l) and GlutaMAX were used to measure OCR at basal respiration stage. After injection of ATP synthase inhibitor oligomycin (1 μmol/l), mitochondrial uncoupler Carbonyl cyanide-4 (trifluoromethoxy) phenylhydrazone (FCCP, 5 μmol/l) and respiratory chain inhibitor antimycin and rotenone (1 μmol/l), real-time OCR was measured to indicate mitochondrial function. All ECAR and OCR values were normalized to cell number and are shown as fold change relative to basal levels.

Metabolite Extraction and Mass Spectrometry-based Analysis—Metabolites were extracted from 2×10^6 cells per sample using the methanol based method. After incubation at 37°C for the indicated time, cells were rinsed with 150 mmol/l ammonium acetate, pH 7.3, and 100 μl cold 80% methanol (Optima* LC/MS, Fisher Scientific) was added to cells. 10 nmol norvaline (Sigma-Aldrich) was added as internal control. Samples were vortexed 3 times over 15 minutes and spun down at top speed for 5 minutes at 4°C. The supernatant was transferred to a new Eppendorf tube, and pellet was resuspended in 50 μl cold 80% methanol for second extraction. Combined 150 μl supernatant was dried on Vacufuge Plus (Eppendorf) at 30°C. Extracted metabolites were stored at −80°C. For mass spectrometry-based analysis, the metabolites were resuspended in 70% ACN and 5 μl used for analysis with a mass spectrometer. The mass spectrometer (Q Exactive, Thermo Scientific) was coupled to an UltiMate3000 RSLCnano HPLC. The chromatography was performed with 5 mmol/l NH_4AcO (pH 9.9) (A) and ACN (B) at a flow rate of 300 μl/min starting at 85% B, going to 5% B at 18 min, followed by an isocratic step to 27 min and reequilibration to 34 min. The separation was achieved on a Luna 3u NH2 100A (150 × 2 mm) (Phenomenex). The Q Exactive was run in polarity switching mode (+3 kV / −2.25 kV). Metabolites were detected based on retention time (t_R) and on accurate mass (± 3 ppm). Metabolite quantification was performed as area-under-the-curve (AUC) with TraceFinder 3.1 (Thermo Scientific). Data were normalized to the number of cells. Log_2-fold changes relative to controls were plotted.

ChIP-seq data analysis—ChIPseq tracks for PAX5, IKZF1, EBF1 and TCF3 antibodies in a normal B cell sample are downloaded from (http://genome.ucsc.edu/ENCODE/dataMatrix/encodeChipMatrixHuman.html). Y-axes represent the normalized number of reads per million for peak summit for each track. The ChIP-seq peaks were called by the MACS peak caller (Zhang et al., 2008) by comparing read density in the ChIP experiment relative to the input chromatin control reads, and shown as bars under each wiggle track. Gene models were shown in UCSC genome browser hg19.

Single-locus quantitative chromatin immunoprecipitation (ChIP)—ChIP was performed as described previously (Chan et al., 2017). Chromatin from fixed patient-derived *Ph*$^+$ B-ALL cells (ICN1) was isolated and sonicated to 100-500 base pair DNA fragments. Chromatin fragments were immunoprecipitated with either IgG (as a control) or anti-Pax5 antibody. Following reversal of crosslinking by formaldehyde, specific DNA sequences were analyzed by quantitative real-time PCR. Primers were designed according to ChIP-seq tracks for PAX5 antibodies in B lymphocytes (ENCODE, Encyclopedia of DNA Elements, GM12878).

CRISPR-Cas9 mediated gene disruption—Patient-derived xenografts (PDX) were transduced with a set of plasmids for inducible Cas9 expression by lentiviral transduction. All Cas9-ZsGreen transduced cells were induced with doxycycline and then sorted for ZsGreen$^+$ using a FACSAria II. After sorting, cells were cultured in tetracycline-free medium and later transduced with gRNAs by lenti-viral transduction. All gRNA-RFP transduced cells were FACS sorted for RFP$^+$ reporter expression. Cas9-RFP expression was induced by doxycycline. ZsGreen$^+$ RFP$^+$ cells were purified for further analysis including target-gene expression measurement and functional assay. For growth competition assay, percentage of targeted cells was calculated as ratios between ZsGreen$^+$RFP$^+$ doublepositive and ZsGreen$^+$ populations. CRISPR-Cas9 plasmid set including all gRNAs for target genes were obtained from transOMIC technologies. The gRNA sequences that were used are listed in Table S6.

Cell viability assays—4×10^4 human or mouse leukemia cells were seeded in a volume of 50 μl in complete growth medium on 96-well plates (Eppendorf). Compounds were added at the indicated concentrations in a total volume of 100 μl per well. After culturing for 3 days, cells were subjected to CCK-8 (Dojindo) or CellTiter-Glo Luminescent Cell Viability Assay (Promega). Medium without cells was used as blank. Relative viability was calculated using baseline values of untreated cells as a reference. For LB-100 (S7537, Selleck Chemicals) and 6-AN (A68203, Sigma-Aldrich) single treatment shown in Figure 7H-I, *Ph*$^+$ ALL xenografts including LAX2, MXP2, PDX2 and BLQ5 (n=4) and myeloid leukemia including KYO-1, EM-2, JURL-MK1 and MV4-11 (n=4) were used.

Quantification and Statistical Analysis

Statistical analysis was performed using GraphPad Prism 7 (GraphPad Software Inc.) and were shown as mean ± SD as indicated. Unpaired 2-tailed Student's t test was used to evaluate difference between two groups and P-values were plotted ($P< 0.05$ was considered statistically significant). For *in vivo* transplantation experiments, the minimal number of mice in each group was calculated through use of the 'cpower' function in the R/Hmisc package. Kaplan-Meier survival analysis was used to estimate OS with GraphPad Prism 7 and log-rank test was used to compare the difference between two groups. For patient overall survival analysis, patients in each dataset were segregated into 2 groups based on 25% highest or 25% lowest mRNA levels of the gene of interest. The datasets used include mantle cell lymphomas (GSE10793, n=71 and http://llmpp.nih.gov/MCL, n = 92), diffuse large B cell lymphoma (DLBCL; GSE10846, n=414), B cell lineage CLL (GSE22726, n=107) and acute myeloid leukemia (https://tcga-data.nci.nih.gov/; n=200).

Log-rank test was used to compare survival differences between patient groups. R package "survival" Version 2.35-8 was used for the survival analysis and Cox proportional hazards regression model in R package for the multivariate analysis (R Development Core Team, 2009). To determine synergism effect of LB-100 and 6-AN in B-ALL and B-cell lymphoma cells, combination index (CI) values were calculated using the CompuSyn software to determine interaction (synergistic, CI<1; additive, CI=1; or antagonistic, CI>1).

Data and Software Availability

The GEO accession number for the gene expression arrays in this study is GSE83742.

Supplementary Material

Refer to Web version on PubMed Central for supplementary material.

ACKNOWLEDGMENTS.

We would like to thank Dr. John S. Kovach (Lixte Biotechnology), Dr. Arthur Riggs (Beckman Research Institute), Dr. Daniel Hodson (University of Cambridge), Dr. David A. Fruman (University of California Irvine). Dr. Michael Farrar (University of Minnesota) and Dr. H. Phillip Koeffler (University of California Los Angeles) and all members of the Muschen laboratory for support and helpful discussions. Research is funded by the NIH/NCI through Outstanding Investigator Award R35CA197628, R01CA137060, R01CA157644, R01CA172558 and R01CA213138 (to M.M.), a Wellcome Trust Senior Investigator Award and a Leukemia and Lymphoma Scholar award (to M.M.), the Howard Hughes Medical Institute HHMI-55108547 (to M.M.), the Norman and Sadie Lee Foundation (for Pediatric Cancer, to M.M.), and the Dr. Ralph and Marian Falk Medical Research Trust (to M.M.), Cancer Research Institute through a Clinic and Laboratory Integration Program grant (to M.M.) and the California Institute for Regenerative Medicine (CIRM) through DISC2-10061. H.J. is supported by Deutsche Forschungsgemeinschaft (SFB1074, P10) and ERC Advanced Grant #694992. M.M. is a Howard Hughes Medical Institute (HHMI) Faculty Scholar.

REFERENCES

Apostolidis SA, Rodríguez-Rodríguez N, Suárez-Fueyo A, Dioufa N, Ozcan E, Crispín JC, Tsokos MG, and Tsokos GC (2016). Phosphatase PP2A is requisite for the function of regulatory T cells. Nat. Immunol. 17, 556–564. [PubMed: 26974206]

Bensaad K, Tsuruta A, Selak MA, Vidal MNC, Nakano K, Bartrons R, Gottlieb E, and Vousden KH (2006). TIGAR, a p53-Inducible Regulator of Glycolysis and Apoptosis. Cell 126, 107–120. [PubMed: 16839880]

Buchner M, Swaminathan S, Chen Z, and Müschen M (2015). Mechanisms of pre-B-cell receptor checkpoint control and its oncogenic subversion in acute lymphoblastic leukemia. Immunol. Rev 263, 192–209. [PubMed: 25510278]

Cairns RA, Harris IS, and Mak TW (2011). Regulation of cancer cell metabolism. Nat. Rev. Cancer 11, 85–95. [PubMed: 21258394]

Chan LN, Chen Z, Braas D, Lee J-W, Xiao G, Geng H, Cosgun KN, Hurtz C, Shojaee S, Cazzaniga V, et al. (2017). Metabolic gatekeeper function of B-lymphoid transcription factors. Nature 542, 479–483. [PubMed: 28192788]

Chen W, Arroyo JD, Timmons JC, Possemato R, and Hahn WC (2005). Cancer-associated PP2A Aalpha subunits induce functional haploinsufficiency and tumorigenicity. Cancer Res. 65, 8183–8192. [PubMed: 16166293]

Chen Z, Shojaee S, Buchner M, Geng H, Lee JW, Klemm L, Titz B, Graeber TG, Park E, Tan YX, et al. (2015). Signalling thresholds and negative B-cell selection in acute lymphoblastic leukaemia. Nature 521, 357–361. [PubMed: 25799995]

Cheung EC, Athineos D, Lee P, Ridgway RA, Lambie W, Nixon C, Strathdee D, Blyth K, Sansom OJ, and Vousden KH (2013). TIGAR Is Required for Efficient Intestinal Regeneration and Tumorigenesis. Dev. Cell 25, 463–477. [PubMed: 23726973]

Chung V, Mansfield AS, Braiteh F, Richards D, Durivage H, Ungerleider RS, Johnson F, and Kovach JS (2017). Safety, Tolerability, and Preliminary Activity of LB-100, an Inhibitor of Protein Phosphatase 2A, in Patients with Relapsed Solid Tumors: An Open-Label, Dose Escalation, First-in-Human, Phase I Trial. Clin. Cancer Res 23, 3277–3284. [PubMed: 28039265]

Düvel K, Yecies JL, Menon S, Raman P, Lipovsky AI, Souza AL, Triantafellow E, Ma Q, Gorski R, Cleaver S, et al. (2010). Activation of a Metabolic Gene Regulatory Network Downstream of mTOR Complex 1. Mol. Cell 39, 171–183. [PubMed: 20670887]

Gutierrez A, Pan L, Groen RWJ, Baleydier F, Kentsis A, Marineau J, Grebliunaite R, Kozakewich E, Reed C, Pflumio F, et al. (2014). Phenothiazines induce PP2A-mediated apoptosis in T cell acute lymphoblastic leukemia. J. Clin. Invest 124, 644–655. [PubMed: 24401270]

Hitosugi T, Zhou L, Elf S, Fan J, Kang H-B, Seo JH, Shan C, Dai Q, Zhang L, Xie J, et al. (2012). Phosphoglycerate Mutase 1 Coordinates Glycolysis and Biosynthesis to Promote Tumor Growth. Cancer Cell 22, 585–600. [PubMed: 23153533]

Hobeika E, Thiemann S, Storch B, Jumaa H, Nielsen PJ, Pelanda R, and Reth M (2006). Testing gene function early in the B cell lineage in mb1-cre mice. Proc. Natl. Acad. Sci. U. S. A. 103, 13789–13794. [PubMed: 16940357]

Hochhaus A, Saussele S, Rosti G, Mahon F-X, Janssen JJWM, Hjorth-Hansen H, Richter J, and Buske C (2017). Chronic myeloid leukaemia: ESMO Clinical Practice Guidelines for diagnosis, treatment and follow-up. Ann. Oncol 28, iv41–iv51. [PubMed: 28881915]

Jeon S-M, Chandel NS, and Hay N (2012). AMPK regulates NADPH homeostasis to promote tumour cell survival during energy stress. Nature 485, 661–665. [PubMed: 22660331]

Kanteti R, Nallasura V, Loganathan S, Tretiakova M, Kroll T, Krishnaswamy S, Faoro L, Cagle P, Husain AN, Vokes EE, et al. (2009). PAX5 is expressed in small-cell lung cancer and positively regulates c-Met transcription. Lab. Investig. 89, 301–314. [PubMed: 19139719]

Lakhanpal GK, Vecchiarelli-Federico LM, Li Y-J, Cui J-W, Bailey ML, Spaner DE, Dumont DJ, Barber DL, and Ben-David Y (2010). The inositol phosphatase SHIP-1 is negatively regulated by Fli-1 and its loss accelerates leukemogenesis. Blood 116, 428–436. [PubMed: 20445019]

Li J, Yen C, Liaw D, Podsypanina K, Bose S, Wang SI, Puc J, Miliaresis C, Rodgers L, McCombie R, et al. (1997). PTEN, a putative protein tyrosine phosphatase gene mutated in human brain, breast, and prostate cancer. Science 275, 1943–1947. [PubMed: 9072974]

Lin R, Elf S, Shan C, Kang H-B, Ji Q, Zhou L, Hitosugi T, Zhang L, Zhang S, Seo JH, et al. (2015). 6-Phosphogluconate dehydrogenase links oxidative PPP, lipogenesis and tumour growth by inhibiting LKB1–AMPK signalling. Nat. Cell Biol 17, 1484–1496. [PubMed: 26479318]

Liu GJ, Cimmino L, Jude JG, Hu Y, Witkowski MT, McKenzie MD, Kartal-Kaess M, Best SA, Tuohey L, Liao Y, et al. (2014). Pax5 loss imposes a reversible differentiation block in B-progenitor acute lymphoblastic leukemia. Genes Dev. 28, 1337–1350. [PubMed: 24939936]

Lu J, Kovach JS, Johnson F, Chiang J, Hodes R, Lonser R, and Zhuang Z (2009). Inhibition of serine/threonine phosphatase PP2A enhances cancer chemotherapy by blocking DNA damage induced defense mechanisms. Proc. Natl. Acad. Sci. U. S. A 106, 11697–11702. [PubMed: 19564615]

Müschen M (2018). Autoimmunity checkpoints as therapeutic targets in B cell malignancies. Nat. Rev. Cancer 18, 103–116. [PubMed: 29302068]

Nemoto S, and Finkel T (2002). Redox regulation of forkhead proteins through a p66shc-dependent signaling pathway. Science 295, 2450–2452. [PubMed: 11884717]

Nogueira V, Park Y, Chen C-C, Xu P-Z, Chen M-L, Tonic I, Unterman T, and Hay N (2008). Akt Determines Replicative Senescence and Oxidative or Oncogenic Premature Senescence and Sensitizes Cells to Oxidative Apoptosis. Cancer Cell 14, 458–470. [PubMed: 19061837]

Patra KC, and Hay N (2014). The pentose phosphate pathway and cancer. Trends Biochem. Sci. 39, 347–354. [PubMed: 25037503]

Pozuelo Rubio M, Peggie M, Wong BHC, Morrice N, and MacKintosh C (2003). 14-3-3s regulate fructose-2,6-bisphosphate levels by binding to PKB-phosphorylated cardiac fructose-2,6-bisphosphate kinase/phosphatase. EMBO J. 22, 3514–3523. [PubMed: 12853467]

Ros S, and Schulze A (2013). Balancing glycolytic flux: the role of 6-phosphofructo-2-kinase/fructose 2,6-bisphosphatases in cancer metabolism. Cancer Metab. 1, 8. [PubMed: 24280138]

Ruediger R, Ruiz J, and Walter G (2011). Human cancer-associated mutations in the Aα subunit of protein phosphatase 2A increase lung cancer incidence in Aα knock-in and knockout mice. Mol. Cell. Biol. 31, 3832–3844. [PubMed: 21791616]

Sangodkar J, Perl A, Tohme R, Kiselar J, Kastrinsky DB, Zaware N, Izadmehr S, Mazhar S, Wiredja DD, O'Connor CM, et al. (2017). Activation of tumor suppressor protein PP2A inhibits KRAS-driven tumor growth. J. Clin. Invest 127, 2081–2090. [PubMed: 28504649]

Sharabi A, Kasper IR, and Tsokos GC (2017). The serine/threonine protein phosphatase 2A controls autoimmunity. Clin. Immunol.

Shojaee S, Chan LN, Buchner M, Cazzaniga V, Cosgun KN, Geng H, Qiu YH, von Minden MD, Ernst T, Hochhaus A, et al. (2016). PTEN opposes negative selection and enables oncogenic transformation of pre-B cells. Nat. Med. 22, 379–387. [PubMed: 26974310]

Swaminathan S, Klemm L, Park E, Papaemmanuil E, Ford A, Kweon S-M, Trageser D, Hasselfeld B, Henke N, Mooster J, et al. (2015). Mechanisms of clonal evolution in childhood acute lymphoblastic leukemia. Nat. Immunol 16, 766–774. [PubMed: 25985233]

Takahashi K, and Yamanaka S (2006). Induction of Pluripotent Stem Cells from Mouse Embryonic and Adult Fibroblast Cultures by Defined Factors. Cell 126, 663–676. [PubMed: 16904174]

Wang SS, Esplin ED, Li JL, Huang L, Gazdar A, Minna J, Evans GA (1998). Alterations of the PPP2R1B gene in human lung and colon cancer. Science. 282: 284–287. [PubMed: 9765152]

Wu Y, Song P, Xu J, Zhang M, and Zou M-H (2007). Activation of protein phosphatase 2A by palmitate inhibits AMP-activated protein kinase. J. Biol. Chem. 282, 9777–9788. [PubMed: 17255104]

Xie H, Ye M, Feng R, and Graf T (2004). Stepwise Reprogramming of B Cells into Macrophages. Cell 117, 663–676. [PubMed: 15163413]

Yan L, Lavin VA, Moser LR, Cui Q, Kanies C, and Yang E (2008). PP2A regulates the proapoptotic activity of FOXO1. J. Biol. Chem 283, 7411–7420. [PubMed: 18211894]

Yang Y, Huang Q, Lu Y, Li X, and Huang S (2012). Reactivating PP2A by FTY720 as a Novel therapy for AML with C-KIT tyrosine kinase domain mutation. J. Cell. Biochem 113, 1314–1322. [PubMed: 22109829]

Yang Z, Shen Y, Oishi H, Matteson EL, Tian L, Goronzy JJ, and Weyand CM (2016). Restoring oxidant signaling suppresses proarthritogenic T cell effector functions in rheumatoid arthritis. Sci. Transl. Med 8, 331ra38.

Young RM, and Staudt LM (2013). Targeting pathological B cell receptor signalling in lymphoid malignancies. Nat. Rev. Drug Discov 12, 229–243. [PubMed: 23449308]

Yusuf I, Zhu X, Kharas MG, Chen J, and Fruman DA (2004). Optimal B-cell proliferation requires phosphoinositide 3-kinase-dependent inactivation of FOXO transcription factors. Blood 104, 784–787. [PubMed: 15069012]

Zhang Y, Liu T, Meyer CA, Eeckhoute J, Johnson DS, Bernstein BE, Nussbaum C, Myers RM, Brown M, Li W, et al. (2008). Model-based Analysis of ChIP-Seq (MACS). Genome Biol. 9, R137. [PubMed: 18798982]

HIGHLIGHTS

- PP2A redirects glucose flux from glycolysis to the PPP to salvage oxidative stress
- B-lymphoid transcription factors repress rate-limiting PPP enzymes in B-cell tumors
- The PPP-agonist TIGAR efficiently rescues B-cells upon genetic ablation of PP2A
- PP2A small molecule inhibition can overcome drug-resistance in B-cell tumors

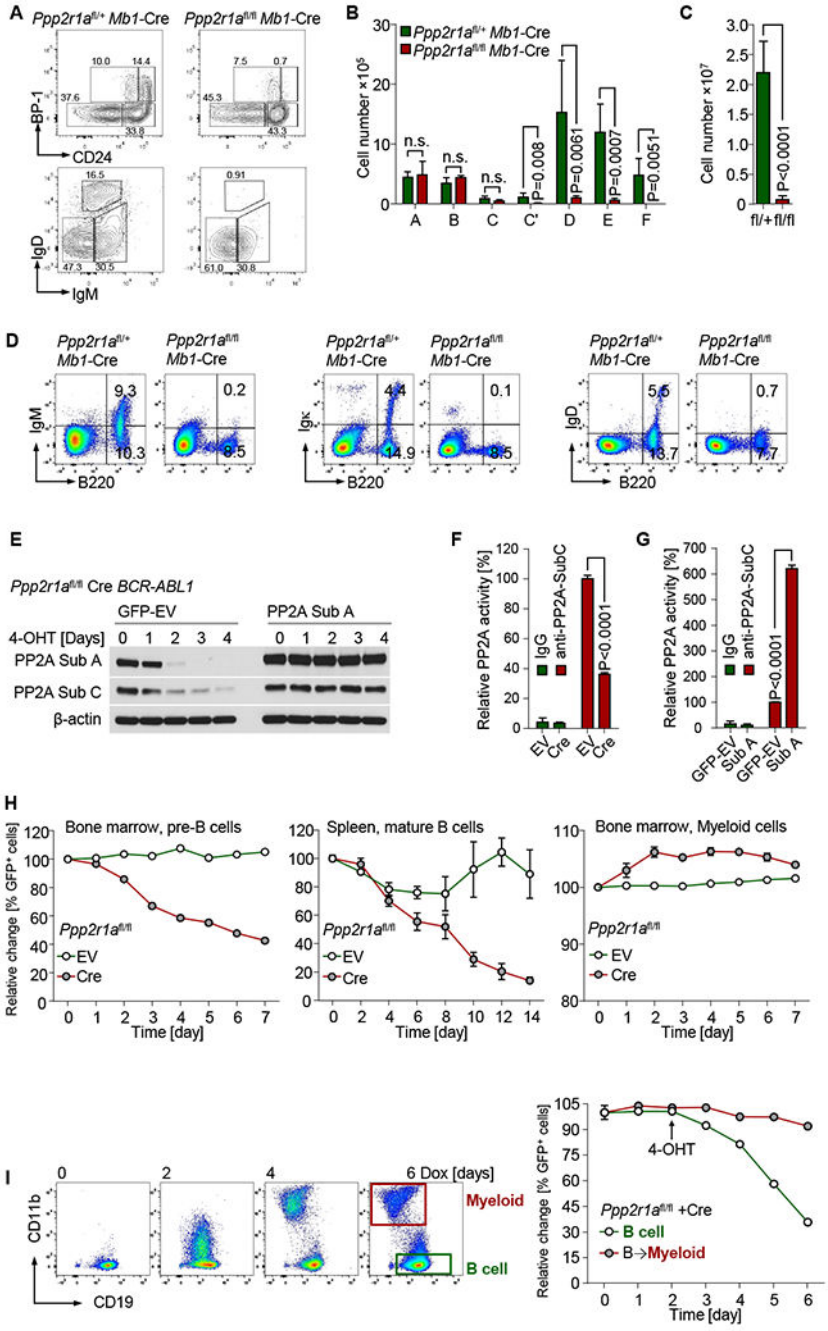

Figure 1: PP2A function is essential for B cell survival.

(A) B cell development in *Ppp2r1a*$^{fl/fl}$ *Mb 1*-Cre mice was examined by flow cytometry. Hardy fractions of B cell subsets isolated from bone marrow were analyzed. Absolute cell numbers were calculated for B cell subsets from bone marrow (B) and spleen (C). Surface staining of BCR components was performed by flow cytometry (D). *Ppp2r1a*$^{fl/fl}$ *BCR-ABL1* ALL cells were transduced with 4-hydroxy-tamoxifen (4-OHT)-inducible Cre-ER^{T2} (Cre) or ER^{T2}-vector (EV). Cells were subsequently transduced with PP2A-subA-IRES-GFP (PP2A Sub A) or GFP-Vector (GFP-EV). (E) PP2A expression in Cre-transduced cells after 4-OHT

treatment was measured by Western blot. PP2A Thr/Ser phosphatase activity was measured in Cre- or EV-transduced cells after 3 days of 4-OHT treatment (F). Cre-GFP^{+} Cre cells transduced with Sub A or GFP-EV were sorted for PP2A-activity measurement after 3-days 4-OHT treatment (G). Bone marrow pre-B cells, splenic B cells and myeloid leukemia cells from *Ppp2r1a*$^{fl/fl}$ mice were transduced with Cre or EV (H). Percentages of GFP^{+} cells were determined by flow cytometry at time points indicated following 4-OHT treatment. (I) *Ppp2r1a*$^{fl/fl}$ *BCR-ABL1* B-ALL cells were transduced with doxycycline (Dox)-inducible C/EBPα (Tet^{On}-*Cebpa*) and subsequently transduced with Cre. Percentages of GFP^{+} cells in B-lymphoid (CD19^{+} CD11b^{-}) and B→myeloid (CD19^{-} CD11b^{+}) populations were measured by flow cytometry at time points indicated following Dox (4-OHT treatment started at time point indicated by arrow). Data are shown as mean ± standard deviation (SD) and representative of at least three independent experiments.

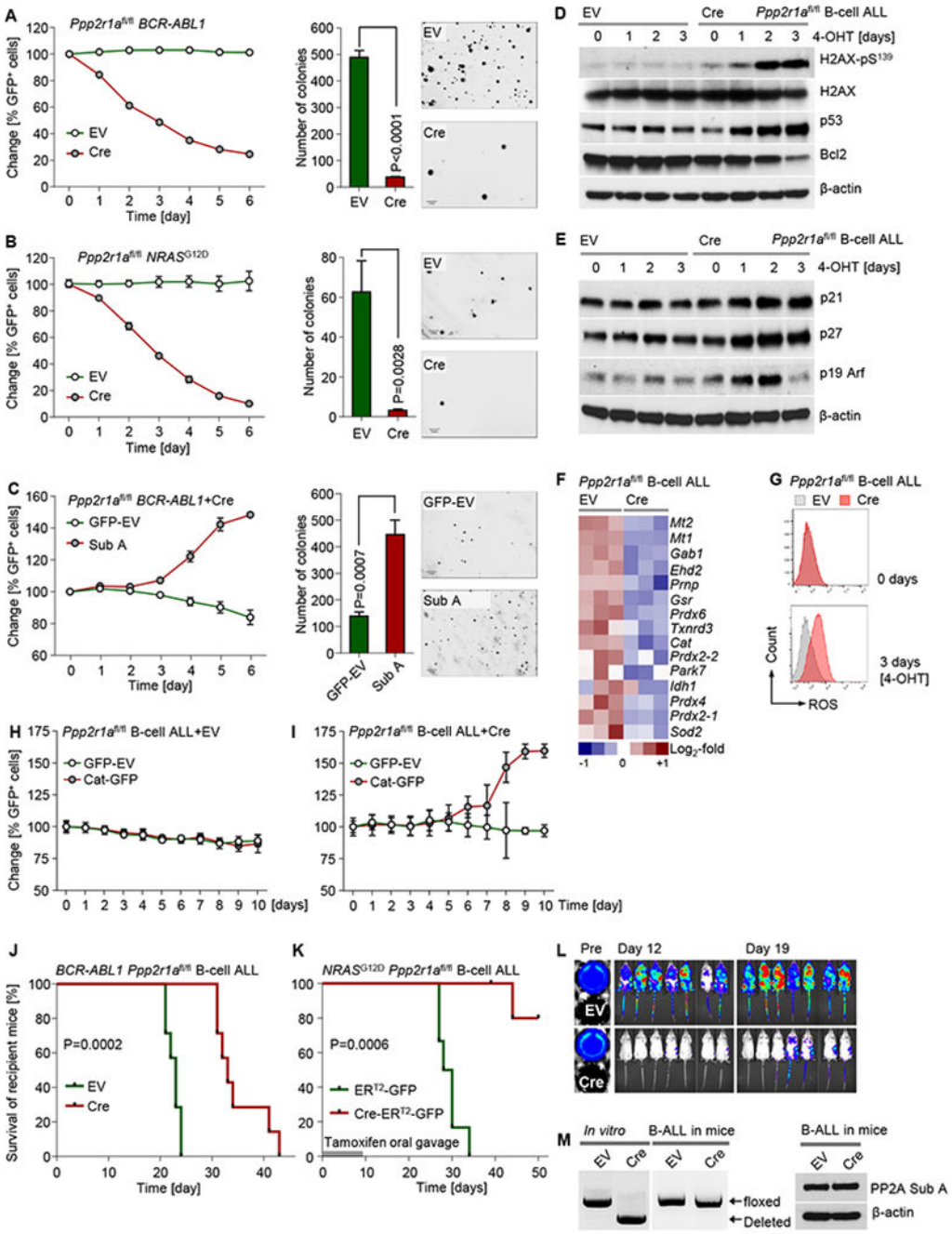

Figure 2: PP2A is required for the survival of BCR-ABL1 and NRAS^{G12D} ALL cells.

Ppp2r1a$^{fl/fl}$ *BCR-ABL1* (A) and *NRAS*^{G12D} B-ALL (B) cells were transduced with Cre-ER^{T2}-IRES-GFP (Cre) or ER^{T2}-IRES-GFP-vector control (EV). Percentages of GFP^{+} cells were measured following 4-OHT treatment. Cre or EV-transduced ALL cells were treated for 3 days with 4-OHT and plated in methylcellulose to perform colony formation assays. Photomicrographs of colonies were taken for colony counting (scale bar indicating 1 mm). (C) The fractions of GFP^{+} *BCR-ABL1* B-ALL cells transduced with Sub A or GFP-EV were measured following 4-OHT treatment. GFP^{+}-sorted cells transduced with Sub A or

GFP-EV were studied by colony formation assay. *Ppp2r1a*$^{fl/fl}$ *BCR-ABL1* B-ALL cells transduced with Cre or EV were treated with 4-OHT. (D) Western blot to measure phosphorylation of H2AX and expression of p53, Bcl2 (D) and p21, p27 and p19 Arf (E) was performed after 4-OHT treatment. (F) A heatmap to depict gene expression changes of antioxidant genes (microarray data; GSE83742) of *Ppp2r1a*$^{fl/fl}$ B-ALL cells after 3-days 4-OHT treatment (Cre-mediated deletion) is shown. (G) ROS levels were measured by flow cytometry as DCF-fluorescence. *Ppp2r1a*$^{fl/fl}$ *BCR-ABL1* ALL cells transduced with EV (H) or Cre (I) were transduced with Catalase-IRES-GFP (*Cat*-GFP) or GFP-vector (EV). Percentages of GFP$^+$ cells were measured following 4-OHT treatment. (J) *Ppp2r1a*$^{fl/fl}$ *BCR-ABL1* ALL cells were labeled with firefly luciferase and transduced with Cre or EV. 2 days after transduction, GFP$^+$ cells were injected intravenously into recipient NSG mice (1×10^6 cells/mouse; 7 mice in each group). B-ALL cell burden was monitored by luciferase bioimaging (L). *Ppp2r1a*$^{fl/fl}$ *NRAS*^{G12D} B-ALL cells were transduced with inducible Cre or EV, sorted for GFP$^+$ cells and injected intravenously into recipient NSG mice (3×10^6 cells/mouse; 6 mice in each group) followed by 7 days of tamoxifen treatment via oral gavage to induce deletion *in vivo* (K). In (J-K), Kaplan-Meier estimates were used to plot the survival probabilities for mice that were transplanted with Cre- and EV-transduced cells. Log-rank test was used to assess statistical significance. In experiment (J), mice that showed signs of illness from leukemia were sacrificed to collect splenic B-ALL cells. GFP$^+$ cells from recipient mice were used for PCR and Western blot to determine *Ppp2r1a* genotype and PP2A expression, respectively (M). Except survival analyses, other experimental data are shown as mean ± standard deviation (SD) and representative of at least three independent experiments.

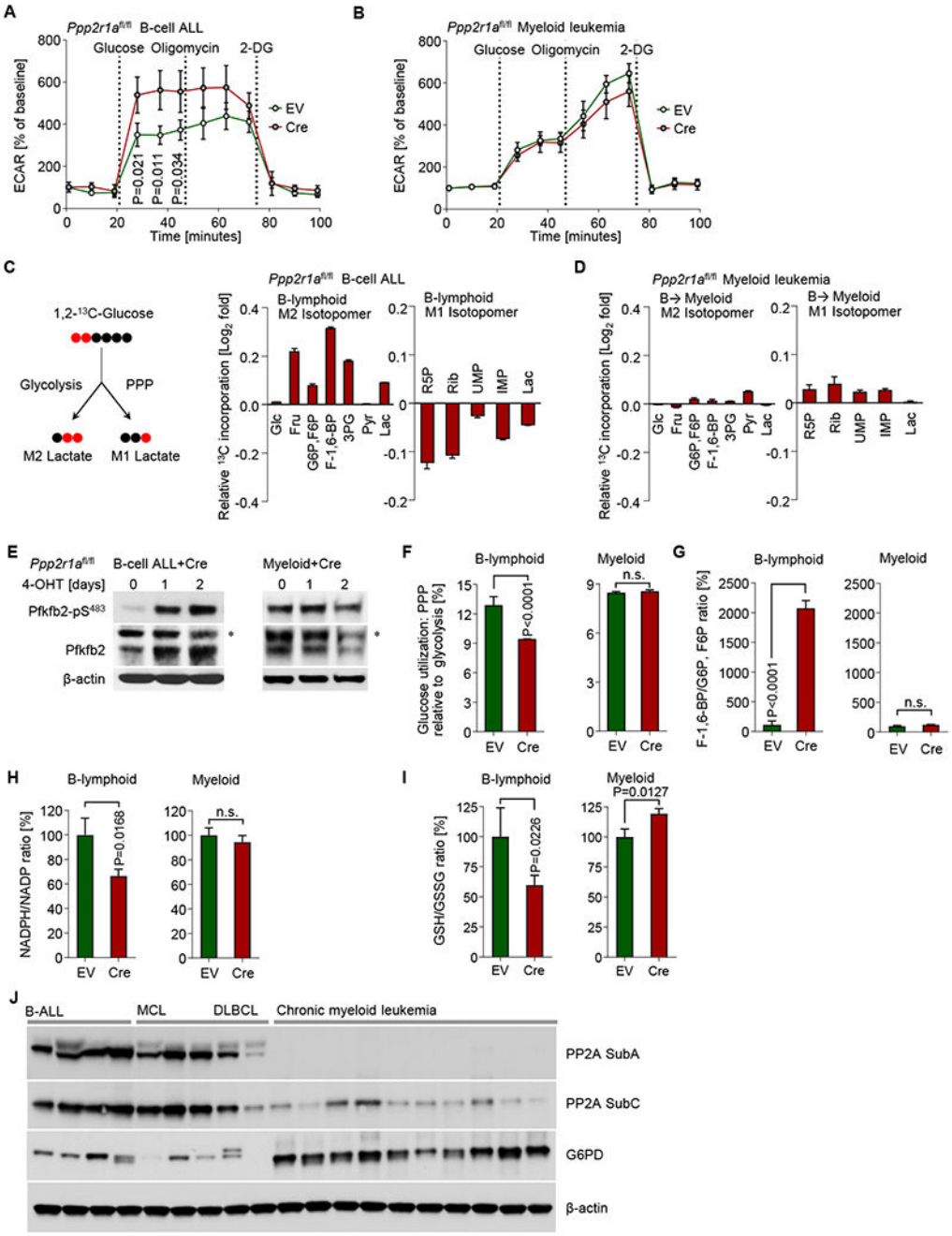

Figure 3: PP2A is essential in B-lymphoid but not myeloid cells to balance glucose carbon utilization via glycolysis and PPP

Extracellular acidification rates (ECAR) were measured in (A) B-lymphoid and (B) myeloid *Ppp2r1a*$^{fl/fl}$ *BCR-ABL1* leukemia cells that were transduced with Cre-ER^{T2} (Cre) or ER^{T2}-vector (EV). Cells were treated with 4-OHT for 2 days prior to ECAR measurements. (C-D) *Ppp2r1a*$^{fl/fl}$ *BCR-ABL1* ALL cells (B-lymphoid) were cultured with 25 mmol/l 1,2-2^{13} C D-glucose for 24 hours, then harvested to extract metabolites for LC-MS based profiling. *Ppp2r1a*$^{fl/fl}$ *BCR-ABL1* ALL cells carrying Tet^{On}-*Cebpa* were transduced with Cre or EV and were treated for 5-days with Dox for B→myeloid reprogramming. Cre-induced changes

of cellular amounts of metabolites that were utilized in glycolysis (M2 ^{13}C isotopomer) or the pentose phosphate pathway (PPP; M1 ^{13}C isotopomer) are shown on a Log_2-fold scale (Cre relative to EV) in B-lymphoid (C) and B→myeloid (D) cells. Phosphorylation levels of Pfkfb2 at S-483 were measured by Western blot in *Ppp2r1a*$^{fl/fl}$ B-lymphoid and myeloid leukemia cells after 4-OHT treatment for Cre-mediated deletion of *Ppp2r1a*. Asterisks denote non-specific bands. (F) Cellular lactate M1/M2 ratio is measured from metabolites profiling data and indicates the relative amount of glucose carbon utilization via PPP and glycolysis pathways, respectively. Relative cellular F1,6BP/G6P, F6P (G) and GSH/GSSG ratios (I) were calculated in B-lymphoid and B→myeloid cells. (H) Relative NADPH/NADP ratios were measured in *Ppp2r1a*$^{fl/fl}$ B-lymphoid and myeloid cells after 2-days 4-OHT treatment for Cre-mediated deletion of *Ppp2r1a*. (J) Western blot to compare PP2A and G6PD expression in patient-derived B-ALL (n=4; MXP2,LAX2, PDX2 and BLQ5), mantle cell lymphoma (MCL; n=3; BOS4, BOS5 and BOS6), diffuse large B cell lymphoma (DLBCL; n=2; BOS10 and BOS12), and chronic myeloid leukemia (n=10; Table S4) samples. Data are shown as mean ± standard deviation (SD) and representative of at least three independent experiments.

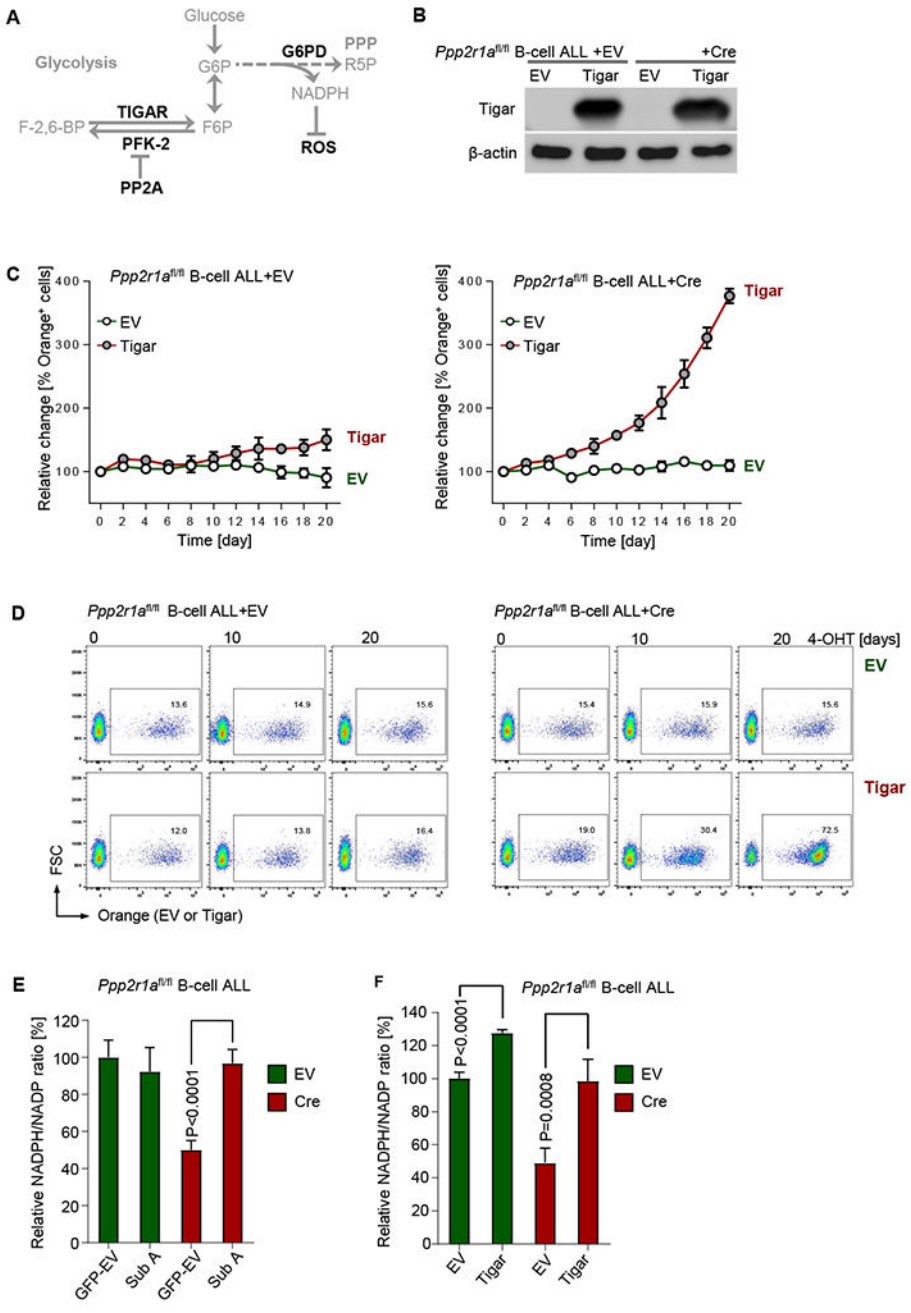

Figure 4: The fructose-2,6-bisphosphate 2-phosphatase TIGAR rescues cell death upon PP2A-deletion

(A) Schematic diagram of TIGAR and PP2A in balancing glucose carbon flux via glycolysis and PPP. (B) *Ppp2r1a*$^{fl/fl}$ *BCR-ABL1* B-ALL cells carrying inducible Cre or EV were subsequently transduced with Tigar-IRES-Orange (Tigar) or Orange-empty vector (EV). Tigar expression was measured by Western blot. (C) Percentages of Orange^{+} B-ALL cells were monitored in a competitive growth assay following 4-OHT treatment. Representative FACS plots are shown at the times indicated (D). (E) *Ppp2r1a*$^{fl/fl}$ B-ALL cells carrying inducible Cre or EV were transduced with vectors for reconstitution or overexpression of

PP2A Sub A (Sub A) or GFP-EV and assayed for cellular NADPH/NADP ratios after 2-days of 4-OHT treatment for inducible activation of Cre or EV for deletion of *Ppp2r1a*. Likewise, Orange^{+} *Ppp2r1a*$^{fl/fl}$ B-ALL cells carrying inducible Cre or EV were transduced with Tigar or EV and assayed for cellular NADPH/NADP ratios after 2-days 4-OHT treatment (F). Data are shown as mean ± standard deviation (SD) and representative of at least three independent experiments.

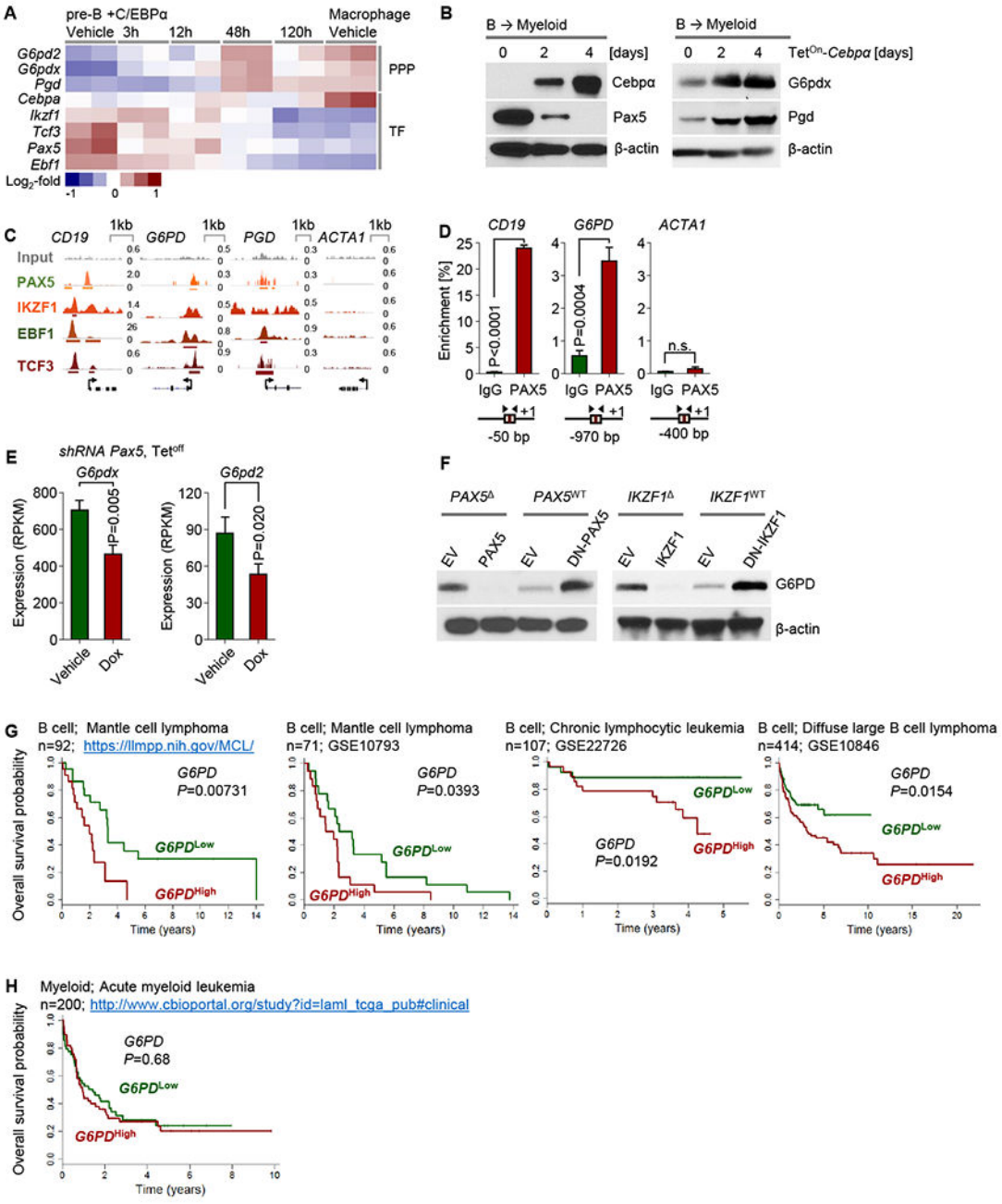

Figure 5: B cell-specific transcriptional repression of rate-limiting PPP enzymes

(A) Gene expression changes in response to Dox-inducible *Cebpa*-mediated reprogramming of mouse pre-B cells into myeloid cells (GSE32330) as a heatmap. (B) Murine B-cell ALL cells were transduced with Tet^{On}-*Cebpa* and induced with Dox. Western blots measuring Cebpα, Pax5, G6pdx and Pgd expression after Dox induction are shown. (C) ChIP-seq data for promoter-binding of transcription factors in human B cells (ENCODE GM12878) of *G6PD* and *PGD* are shown. *CD19* and *ACTA1* are shown as positive and negative controls for PAX5, respectively. (D) Single-locus quantitative ChIP in patient-derived *Ph*$^{+}$ ALL cells

(ICN1) was performed to confirm the recruitment of PAX5 to the *G6PD* promoter. (E) *G6pdx* and *G6pd2* expression from RNA-seq data (GSE52870) of Dox-induced Pax5 restoration in a mouse model for B-ALL is shown as bar graph. (F) Patient-derived Ph^+ ALL cells (MXP2 and ICN1) carrying *PAX5* deletions ($PAX5^{\Delta}$) or wildtype ($PAX5^{WT}$) alleles were transduced with wildtype PAX5 or dominant-negative *ETV6-PAX5* (DN-PAX5) respectively. $IKZF1^{\Delta}$ (BV173) and $IKZF1^{WT}$ (ICN1) Ph^+ ALL cells were transduced with wildtype IKZF1 or DN-IKZF1 respectively. Protein lysates were used for Western blots to measure G6PD expression. Patients with MCL, DLBCL and CLL (G) or AML (H) were divided into two groups based on 25% highest- or lowest- mRNA levels of *G6PD*. Overall survival of patients was assessed in the two groups by Kaplan–Meier analysis. Log-rank test was used to assess statistical significance. Besides clinical outcome studies, experimental data are shown as mean ± standard deviation (SD) and representative of at least three independent experiments.

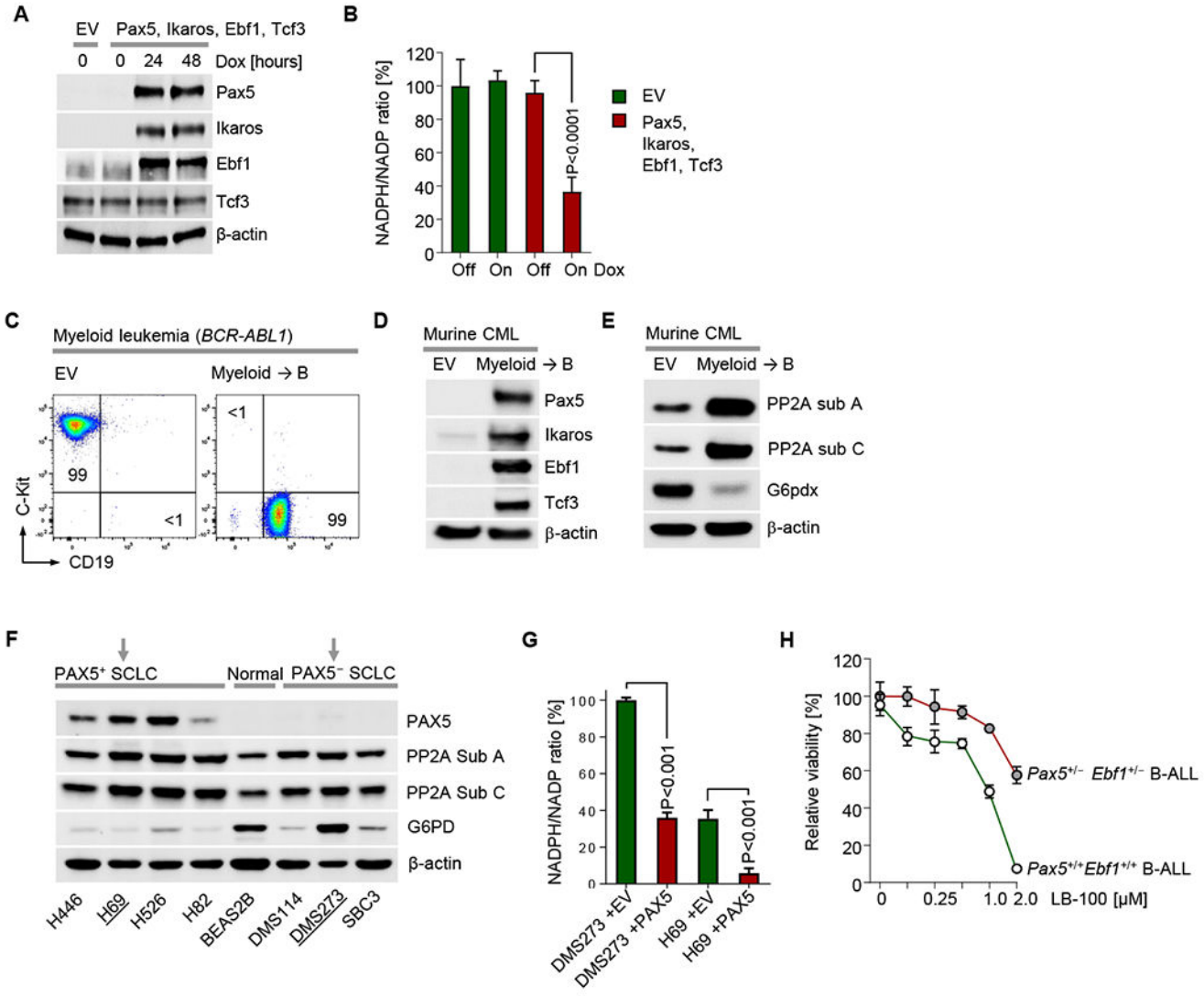

Figure 6: Transcription factors that determine B cell identity regulate activity of the pentose phosphate pathway and dependency on PP2A

(A) Human embryonic kidney cells (HEK-293) were transduced with a polycistronic doxycycline (Dox)-inducible vector to express the B-lineage transcription factors Pax5, Ikaros, Ebf1 and Tcf3, as confirmed by Western blot after Dox treatment for the times indicated. (B) Relative NADPH/NADP ratios were measured before and after 24 hours of Dox-induction of the polycistronic vector (Pax5, Ikaros, Ebf1 and Tcf3) or EV. (C) Murine myeloid leukemia cells were transduced with the inducible polycistronic vector for myeloid→B cell reprogramming. Phenotypic changes were monitored by flow cytometry 48 hours after induction of Dox and expression of Pax5, Ikaros, Ebf1 and Tcf3 was confirmed by Western blot. (E) In the same cells, protein levels for PP2A Sub A, PP2A Sub C and G6pdx were measured by Western blot. (F) Human small cell lung cancer (SCLC) and normal lung epithelial (BEAS2B) cell lines were used to compare PAX5, PP2A and G6PD expression by Western blot. (G) NADPH/NADP ratios were measured in $PAX5^{+}$ and $PAX5^{-}$

SLCL cell lines and upon expression of PAX5 or EV. (H) Murine *Pax5*$^{+/-}$*Ebf1*$^{+/-}$ *BCR-ABL1* B-ALL cells were treated with the PP2A-inhibitor LB-100 at the concentrations indicated. Dose response curves depicting relative cell viability after 72 hours are depicted. Data are shown as mean ± standard deviation (SD) and representative of at least three independent experiments.

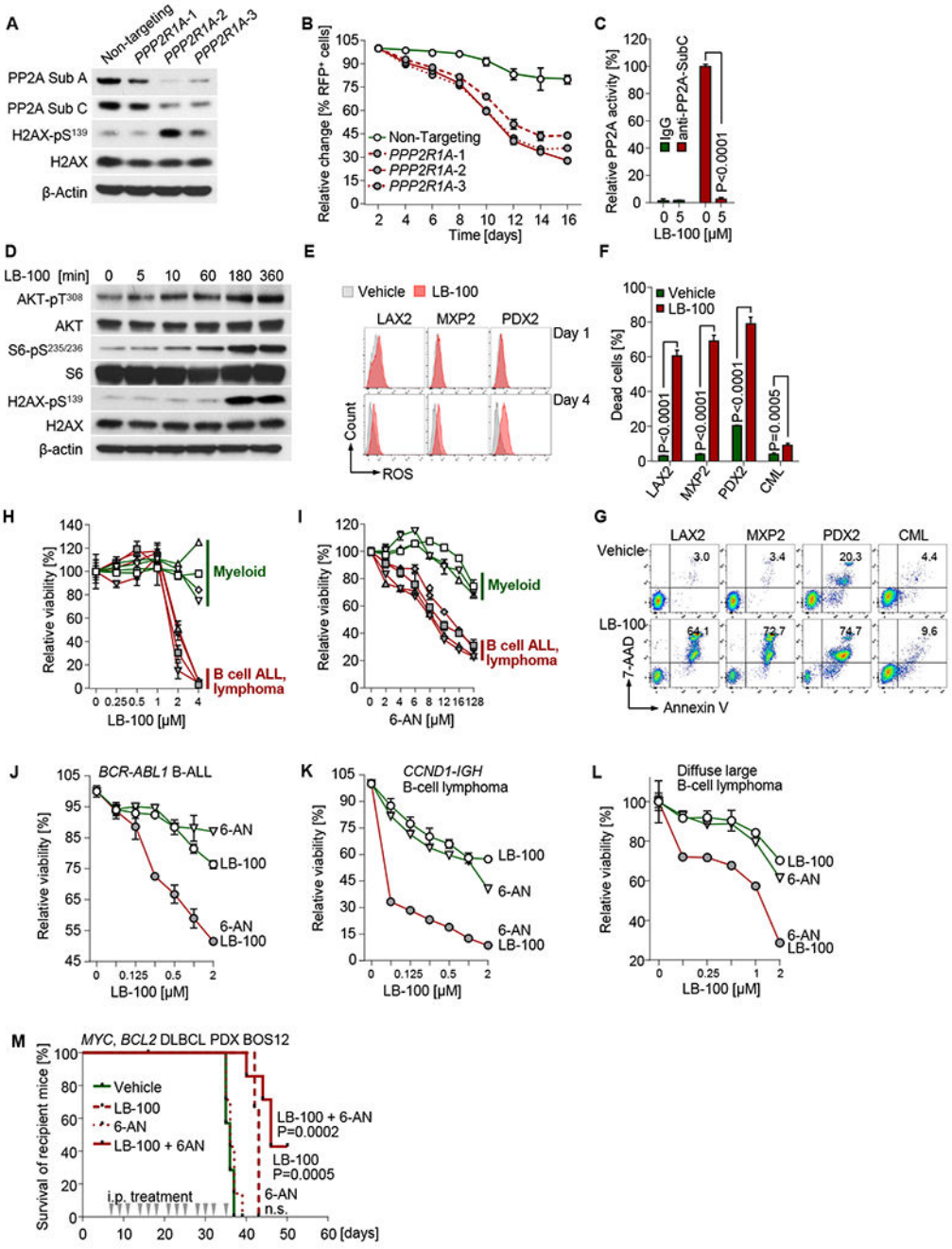

Figure 7: Target validation of PP2A and the PPP in human B cell malignancies

(A) Patient-derived *Ph*$^{+}$ ALL xenograft (PDX2) cells were used for doxycycline (Dox)-inducible CRISPR-Cas9 mediated gene disruption of *PPP2R1A* (3 different gRNAs were used). Western blot was performed to measure expression of PP2A and phosphorylation of H2AX after 3 days of Dox-treatment. (B) Percentages of targeted cells were measured following Dox-treatment. (C) Patient-derived *Ph*$^{+}$ ALL xenograft (LAX2) cells were treated with the PP2A inhibitor LB-100 (5 μmol/l) for 12 hours. Cell lysates were assayed for PP2A Thr/Ser phosphatase activity assay. (D) The same cells were cultured with 2 μmol/L LB-100

and harvested at time points indicated. Western blot was performed to measure phosphorylation of AKT, S6 and H2AX. (E) Intracellular ROS levels were measured in patient-derived *Ph*$^+$ ALL xenografts cells on days 1 and 4 of treatment with LB-100 (2 μmol/L). (F) Cell viability measurements of human B-lymphoid *Ph*$^+$ ALL (LAX2, MXP2, PDX2) and myeloid leukemia cells (JURL-MK1) cells after 4-days of treatment with 2 μmol/L LB-100 are plotted. Representative flow cytometry plots are shown (G). (H-I) Relative cell viabilities were measured after treatment of LB-100 (H) or 6-AN (I) for 72 hours with gradients of concentrations as indicated in B-lineage *Ph*$^+$ ALL (LAX2, MXP2, PDX2 and BLQ5; n=4) and myeloid leukemia (KYO-1, EM-2, JURL-MK1 and MV4-11; n=4) cells. Y-axis shows percentages of viable cells relative to vehicle-treated cells (set to 100%). (J) Patient-derived *Ph*$^+$ ALL (PDX2) cells, (K) mantle cell lymphoma cells (SP-53) and (L) diffuse large B-cell lymphoma cells (OCI-Ly10) were treated with LB-100, 6-AN or a combination of both compounds for 72 hours. Relative cell viability was assessed to measure synergistic effect of combination treatment. (M) Patient-derived diffuse large B cell lymphoma cells (BOS12) were intravenously injected to recipient NSG mice (3×10^6 cells/mouse; 7 mice in each group). Intraperitoneal injection of LB-100 (1.5 mg/kg), 6-AN (1 mg/kg) or combination (1.5 mg/kg LB-100 + 1 mg/kg 6-AN) started 7 days after cell injection at indicated time points. Kaplan-Meier survival curves are shown. Log-rank test was used to assess statistical significance of each treated group compared to vehicle group. Except for Kaplan-Meier survival analyses, other experimental data are shown as mean ± standard deviation (SD) and representative of at least three independent experiments.

KEY RESOURCES TABLE

REAGENT or RESOURCE	SOURCE	IDENTIFIER
Antibodies		
Monoclonal (C4) anti-β-actin	Santa Cruz Biotechnology	Cat# sc-47778
Monoclonal (81G5) anti-PP2A subunit A	Cell Signaling Technology	Cat# 2041
Monoclonal (52F8) anti-PP2A subunit C	Cell Signaling Technology	Cat# 2259
Polyclonal anti-STAT5	Cell Signaling Technology	Cat# 9363
Monoclonal (D47E7) anti-p-STAT5 (Y694)	Cell Signaling Technology	Cat# 4322
Polyclonal anti-Erk	Cell Signaling Technology	Cat# 9102
Monoclonal (D13.14.4E) anti-p-Erk (T202/Y204)	Cell Signaling Technology	Cat# 4370
Polyclonal anti-Akt	Cell Signaling Technology	Cat# 9272
Monoclonal (D25E6) anti-p-Akt (T308)	Cell Signaling Technology	Cat# 13038
Monoclonal (C29H4) anti-FoxO1	Cell Signaling Technology	Cat# 2880
Polyclonal anti-p-FoxO1 (T24)	Cell Signaling Technology	Cat# 9464
Polyclonal anti-p-FoxO1 (S256)	Cell Signaling Technology	Cat# 9461
Monoclonal (75D8) anti-FoxO3a	Cell Signaling Technology	Cat# 2497
Monoclonal (D18H8) anti-p-FoxO3a (S253)	Cell Signaling Technology	Cat# 13129
Monoclonal (2217) anti-S6	Cell Signaling Technology	Cat# 2217
Monoclonal (4856) anti-p-S6 (S235/236)	Cell Signaling Technology	Cat# 4856
Polyclonal anti-p70 S6 kinase	Cell Signaling Technology	Cat# 9202
Polyclonal anti-p-p70 S6 kinase (T389)	Cell Signaling Technology	Cat# 9205
Polyclonal anti-PFKFB2	Milipore	Cat# 07-1530
Monoclonal (D4R1W) anti-p-PFKFB2 (S483)	Cell Signaling Technology	Cat# 13064
Polyclonal anti-H2AX	Abcam	Cat# Ab10475
Polyclonal anti-p-H2AX (S139)	Abcam	Cat# Ab2893
Monoclonal (2524) anti-p53	Cell Signaling Technology	Cat# 2524
Monoclonal (C-2) anti-Bcl2	Santa Cruz Biotechnology	Cat# sc-7382
Polyclonal anti-p21	Santa Cruz Biotechnology	Cat# sc-397
Monoclonal (F-8) anti-p27	Santa Cruz Biotechnology	Cat# sc-1641
Polyclonal anti-p19 ARF (mouse)	Abcam	Cat# ab80
Polyclonal anti-G6PD	Cell Signaling Technology	Cat# 8866
Monoclonal (G-2) anti-PGD	Santa Cruz Biotechnology	Cat# sc-398977
Polyclonal anti-TIGAR	Invitrogen	Cat# PA5-23053
Polyclonal anti-Pax5 (for ChIP)	Santa Cruz Biotechnology	Cat# sc-1974
Monoclonal anti-Pax5 (for western blot)	Cell Signaling Technology	Cat# 8970S
Monoclonal anti-Ikaros	Cell Signaling Technology	Cat# 14859S
Monoclonal anti-EBF1	Abcam	Cat# ab108369
Poly clonal anti-E2A (TCF3)	Santa Cruz Biotechnology	Cat# sc-349
Monoclonal (1D3) anti-Mouse CD19	BD Biosciences	Cat# 557655

REAGENT or RESOURCE	SOURCE	IDENTIFIER
Monoclonal (RA3-6B2) anti-Mouse CD45R	Biolegend	Cat# 103224
Monoclonal (M1/70) anti-Mouse CD11b	Biolegend	Cat# 101208
Monoclonal (6C3) anti-Mouse Ly-51 (BP-1)	Biolegend	Cat# 108305
Monoclonal (M1/69) anti-Mouse CD24	BD Biosciences	Cat# 562477
Monoclonal (11-26c.2a) anti-Mouse IgD	Biolegend	Cat# 405716
Monoclonal (R6-60.2) anti-Mouse IgM	BD Biosciences	Cat# 550881
Monoclonal (JC5-1) anti-Mouse Ig Light Chain, λ	Southern Biotech	Cat# 1175-09
Monoclonal (187.1) anti-Mouse Ig Light Chain, κ	BD Biosciences	Cat# 562476
Monoclonal (17A2) anti-Mouse CD3	Biolegend	Cat# 555275
Monoclonal (RM4-5) anti-Mouse CD4	BD Biosciences	Cat# 553049
Monoclonal (53-6.7) anti-Mouse CD8a	BD Biosciences	Cat# 553033
Monoclonal (PK136) anti-Mouse NK1.1	BD Biosciences	Cat# 553165
Monoclonal (RB6-8C5) anti-Mouse Gr-1 (Ly-6G/Ly-6C)	BD Biosciences	Cat# 553128
Monoclonal (TER-119) anti-Mouse TER-119	BD Biosciences	Cat# 553673
Monoclonal (2B8) anti-Mouse CD117 (c-Kit)	BD Biosciences	Cat# 553356
Monoclonal (HIB19) anti-Human CD19	BD Biosciences	Cat# 555413
Biological Samples		
Patient-derived pre-B ALL samples, see Table S2	Müschen Laboratory	http://lymphoblasts.org/
Patient-derived B-cell lymphoma samples, see Table S3	Müschen Laboratory	http://lymphoblasts.org/
Patient-derived B-cell lymphoma samples, see Table S3	Weinstock Laboratory	https://www.proxe.org/
Patient-derived chronic myeloid leukemia (CML) samples, see Table S4	Thomas Ernst and Andreas Hochhaus	Jena University Hospital, Germany
Chemicals, Peptides, and Recombinant Proteins		
Imatinib	LC Laboratories	Cat# I-5577
Idelalisib	Selleck Chemicals LLC	Cat# S2226
Rapamycin	Sigma-Aldrich	Cat# 37094
4-hydroxy-tamoxifen	Sigma-Aldrich	Cat# 94873
Doxycycline	Clontech Laboratories	Cat# 631311
Tamoxifen	Sigma-Aldrich	Cat# 85256
LB-100	Selleck Chemicals LLC	Cat# S7537
6-AN	Sigma-Aldrich	Cat# A68203
Critical Commercial Assays		
Click-iT EdU Flow Cytometry Assay Kit	Life Technologies	Cat# C10635
PP2A Immunoprecipitation Phosphatase Assay Kit	Millipore	Cat# 17-313
APC Annexin V	BD Biosciences	Cat# 550474
Guava TUNEL Kit for Flow Cytometry	Millipore	Cat# 4500-0121
Phospho-Kinase Antibody Array	R&D Systems	Cat# ARY003B
NADP/NADPH Assay Kit	Abcam	Cat# Ab65394
Amplex™ Red Glucose/Glucose Oxidase Assay Kit	Thermo Fisher Scientific	Cat# A22189

REAGENT or RESOURCE	SOURCE	IDENTIFIER
L-Lactate Assay Kit	Cayman Chemical	Cat# 700510
ATP Bioluminescence Assay Kit CLS II	Roche	Cat# 11699709001
Seahorse XF Glycolysis Stress Test Kit	Agilent Technologies	Cat# 103020-100
Seahorse XF Cell Mito Stress Test Kit	Agilent Technologies	Cat# 103015-100
Deposited Data		
Affymetrix Gene Chip expression data, *Ppp2r1a*-deletion	This paper	GSE83742
Affymetrix Gene Chip expression data, CEBPA-mediated reprogramming	Dr. Thomas Graf	GSE32330
Chromatin IP sequencing data	ENCODE	GM12878
Expression profiling by high throughput sequencing, Pax5 restoration	Dr. Ross A. Dickins	GSE52870
Affymetrix Gene Chip expression data, mantle cell lymphoma	Dr. Andreas Rosenwald	GSE10793
Affymetrix Gene Chip expression data, mantle cell lymphoma	LLMPP	http://llmpp.nih.gov/MCL
Affymetrix Gene Chip expression data, diffuse large B cell lymphoma (DLBCL)	Dr. Louis M. Staudt	GSE10846
Affymetrix Gene Chip expression data, chronic lymphocytic leukemia (B-CLL)	Dr. Tobias Herold	GSE22762
Affymetrix Gene Chip expression data, acute myeloid leukemia	TCGA	N/A
Experimental Models: Cell Lines		
KASUMI-2	DSMZ	Cat# ACC 526
KYO-1	DSMZ	Cat# ACC 601
EM-2	DSMZ	Cat# ACC 135
JURL-MK1	DSMZ	Cat# ACC 532
KCL-22	DSMZ	Cat# ACC 519
K-562	ATCC	Cat# CCL-243
MV4-11	ATCC	Cat# CRL-9591
MOLM-13	DSMZ	Cat# ACC 554
U-937	ATCC	Cat# CRL-1593.2
MEG-01	ATCC	Cat# CRL-2021
BV-173	DSMZ	Cat# ACC 20
OCI-Ly10	From Dr. Daniel Hodson	CVCL_8795
SP-53	From Dr. Ngo Vu	CVCL_C122
H446	ATCC	Cat# HTB-171
H69	ATCC	Cat# HTB-119
H526	ATCC	Cat# CRL-5811
H82	ATCC	Cat# HTB-175
DMS114	ATCC	Cat# CRL-2066
DMS273	Sigma	Cat# 95062830
SBC3	JCRB	Cat# JCRB0818
BEAS2B	ATCC	Cat# CRL-9609
HEK 293T	Clontech Laboratories	Cat# 632180

REAGENT or RESOURCE	SOURCE	IDENTIFIER
Experimental Models: Organisms/Strains		
Mouse: *Ppp2r1a*$^{fl/fl}$: *Ppp2r1a*$^{tm1.1Wltr}$	The Jackson Laboratory	Cat# 017441
Mouse: *Mb1*-Cre: *Cd79a*$^{tm1(cre)Reth}$	The Jackson Laboratory	Cat# 020505
Mouse: NSG: NOD.Cg-*Prkdc*^{scid} *Il2rg*^{tm1Wjl}/SzJ	The Jackson Laboratory	Cat# 005557
Mouse: *Pax5*$^{+/-}$ *Ebf1*$^{+/-}$	Dr. Michael Farrar	N/A
Oligonucleotides		
Primers for genotyping and qChIP, see Table S6	Eurofins Scientific	N/A
sgRNA for CRISPR-Cas9 mediated gene disruption, see Table S6	transOMIC Technologies	TEVH-1259980 TEVH-1192838 TEVH-1125696
Recombinant DNA		
MSCV-BCR-ABL1	Rick Van Etten Laboratory	BCR-ABL1 (p210)
MSCV-BCR-ABL1-IRES-Neo	Rick Van Etten Laboratory	BCR-ABL1 (p210)
MSCV-NRAS^{G12D}-Puro	Müschen Laboratory	NRAS^{G12D}
MSCV-Luc-Puro	Müschen Laboratory	Firefly luciferase
pCL6-Luc-Blast	Müschen Laboratory	Firefly luciferase
MSCV-IRES-GFP	Müschen Laboratory	GFP
MSCV-Cre-IRES-GFP	Müschen Laboratory	GFP
MSCV-PPP2R1A-IRES-GFP	Müschen Laboratory	PP2A subunit A
MSCV-CAT-IRES-GFP	Müschen Laboratory	Catalase
MSCV-ER^{T2}-IRES-Puro	Müschen Laboratory	Puromycin
MSCV-Cre-ER^{T2}-IRES-Puro	Müschen Laboratory	GFP
MSCV-ER^{T2}-IRES-GFP	Müschen Laboratory	GFP
MSCV-Cre-ER^{T2}-IRES-Puro	Müschen Laboratory	GFP
MSCV-mG6pdx-IRES-GFP	Müschen Laboratory	G6PD
MSCV-G6PD-IRES-GFP	Müschen Laboratory	G6PD
MSCV-FoxO1-ADA-IRES-GFP	Müschen Laboratory	FOXO1
pMIThy1.1(CD90)	From Dr. David A. Fruman	CD90
pMIThy1.1(CD90)-FoxO3a-CA	From Dr. David A. Fruman	CD90
pCGDNsam-IRES-Kusabira Orange	From Dr. H. Phillip Koeffler	K-Orange
pCGDNsam-Tigar-IRES-Kusabira Orange	Müschen Laboratory	K-Orange
pRetroX-Tet3G-Neo	Clontech Laboratories	Cat# 631188
pRetroX-TRE3G-c/EBPα-Puro	Thomas Graf, Barcelona	CEBPA
pRetroX-TRE3G-Pax5-Ikaros-Ebf1-Tcf3	Müschen Laboratory	Ali's vector
pCL6-ER^{T2}-IRES-GFP	Hassan Jumaa Laboratory	GFP
pCL6-PAX5-ER^{T2}-IRES-GFP	Müschen Laboratory	PAX5
pCL6-PAX5-ETV6-ER^{T2}-IRES-GFP	Müschen Laboratory	PAX5-ETV6
pLVX-TRE3G-GFP	Clontech Laboratories	Cat# 631361
pLVX-TRE3G-IKZF1-GFP	Hilde Schjerven laboratory, UCSF	Ikaros
pLVX-TRE3G-IK6-GFP	Hilde Schjerven laboratory, UCSF	Dominant-negative Ikaros

REAGENT or RESOURCE	SOURCE	IDENTIFIER
pTOL-hCMV-TET3G-Hygro	transOMIC Technologies	Cat# CCIHS1001
pCLIP-TRE3G-Cas9-ZsGreen	transOMIC Technologies	Cat# CCIMS1001
pCLIP-hCMV-gRNA-tRFP	transOMIC Technologies	Cat# CCIRS1001
Software and Algorithms		
BRB Array Tool	http://linus.nci.nih.gov/BRB-ArrayTools.html	
Gene Cluster	http://www.eisenlab.org/software.html	
Java Treeview	http://jtreeview.sourceforge.net/	
Gene Set Enrichment Analysis (GSEA)	http://software.broadinstitute.org/gsea/index.jsp	
CompuSyn	http://www.combosyn.com/	
R package “survival” Version 2.35-8	N/A	
Other		